

2

AFHAL-TR-88-3102

AD-A208 108



HEAT-TRANSFER AND FRICTION FACTOR DESIGN DATA
FOR ALL-METAL COMPACT HEAT EXCHANGERS

CHRISTINA L. CAIN

VEHICLE SUBSYSTEMS DIVISION
ENVIRONMENTAL CONTROL BRANCH
ADVANCED THERMAL MANAGEMENT GROUP

MARCH 1989

SUMMARY REPORT FOR PERIOD JAN 85 - NOV 87

Approved for public release; distribution unlimited.

DTIC
ELECTE
MAY 18 1989
S H D
Pb

FLIGHT DYNAMICS LABORATORY
AIR FORCE WRIGHT AERONAUTICAL LABORATORIES
AIR FORCE SYSTEMS COMMAND
WRIGHT-PATTERSON AIR FORCE BASE, OH 45433-6553

027

REPORT DOCUMENTATION PAGE

1a. REPORT SECURITY CLASSIFICATION		1b. RESTRICTIVE MARKINGS	
2a. SECURITY CLASSIFICATION AUTHORITY		3. DISTRIBUTION/AVAILABILITY OF REPORT Approved for public release; distribution unlimited.	
2b. DECLASSIFICATION/DOWNGRADING SCHEDULE			
4. PERFORMING ORGANIZATION REPORT NUMBER(S) AFWAL-TR-88-3102		5. MONITORING ORGANIZATION REPORT NUMBER(S)	
6a. NAME OF PERFORMING ORGANIZATION Air Force Wright Aeronautical Laboratories	6b. OFFICE SYMBOL (if applicable) AFWAL/FIEE	7a. NAME OF MONITORING ORGANIZATION	
6c. ADDRESS (City, State, and ZIP Code) Wright-Patterson AFB OH 45433-6553		7b. ADDRESS (City, State, and ZIP Code)	
8a. NAME OF FUNDING/SPONSORING ORGANIZATION	8b. OFFICE SYMBOL (if applicable)	9. PROCUREMENT INSTRUMENT IDENTIFICATION NUMBER	
8c. ADDRESS (City, State, and ZIP Code)		10. SOURCE OF FUNDING NUMBERS	
		PROGRAM ELEMENT NO. 62201F	PROJECT NO. 2402
		TASK NO. 04	WORK UNIT ACCESSION NO. 68
11. TITLE (Include Security Classification) Heat-Transfer and Friction Factor Design Data for All-Metal Compact Heat Exchangers			
12. PERSONAL AUTHOR(S) Cain, Christina L			
13a. TYPE OF REPORT Final	13b. TIME COVERED FROM Jan 85 to Nov 87	14. DATE OF REPORT (Year, Month, Day) March 1989	15. PAGE COUNT 110
16. SUPPLEMENTARY NOTATION			
17. COSATI CODES		18. SUBJECT TERMS (Continue on reverse if necessary and identify by block number)	
FIELD 20	GROUP 13	Heat Exchangers, Compact Heat Exchangers, All-metal Heat Exchangers, Cryogenics, Thermodynamics, Heat Transfer.	
22	02		
19. ABSTRACT (Continue on reverse if necessary and identify by block number) → This report covers analysis and testing Arthur D. Little, Inc conducted under Rotary Reciprocating Refrigerator Development Programs To improve system life, an effort was undertaken to develop all-metal compact heat exchangers to replace existing heat exchangers which contain organic materials. Eliminating organic materials increases system life because outgassing organics can contaminate the helium working fluid and reduce system life. Perforated plate heat exchangers have been found to have inherently low axial conduction and are therefore excellent candidates for cryogenic applications where an all-metal design is required. A total of 11 plate cores were tested; 2 were chemically etched, 1 was mechanically punched, and 8 were manufactured using electron beam drilling. Hole size, percent open area, and plate thickness parameters were varied among the plates. Experimental results were compared to analytical projections and found to differ significantly. The single-blow transient test technique was used to determine the heat transfer coefficients and the isothermal pressure drop test was used to determine friction factors, as a function of Reynolds number.			
20. DISTRIBUTION/AVAILABILITY OF ABSTRACT <input checked="" type="checkbox"/> UNCLASSIFIED/UNLIMITED <input type="checkbox"/> SAME AS RPT. <input type="checkbox"/> DTIC USERS		21. ABSTRACT SECURITY CLASSIFICATION Unclassified	
22a. NAME OF RESPONSIBLE INDIVIDUAL Capt Cain		22b. TELEPHONE (Include Area Code) 513 255 6078	22c. OFFICE SYMBOL AFWAL/FIEE

ABSTRACT

This report covers analysis and testing Arthur D. Little, Inc conducted under Rotary Reciprocating Refrigerator Development Programs. To improve system life, an effort was undertaken to develop all-metal compact heat exchangers to replace existing heat exchangers which contain organic materials. Eliminating organic materials increases system life because outgassing organics can contaminate the helium working fluid and reduce system life. Perforated plate heat exchangers have been found to have inherently low axial conduction and are therefore excellent candidates for cryogenic applications where an all-metal design is required. A total of 11 plate cores were tested; 2 were chemically etched, 1 was mechanically punched, and 8 were manufactured using electron beam drilling. Hole size, percent open area, and plate thickness parameters were varied among the plates. Experimental results were compared to analytical projections and found to differ significantly. The single-blow transient test technique was used to determine the heat transfer coefficients and an isothermal pressure drop test was used to determine friction factors, as a function of Reynolds number.



Accession For	
NTIS GRA&I	<input checked="" type="checkbox"/>
DTIC TAB	<input type="checkbox"/>
Unannounced	<input type="checkbox"/>
Justification	
By _____	
Distribution/	
Availability Codes	
Dist	Avail and/or Special
A-1	

TABLE OF CONTENTS

SECTION	PAGE
I Introduction	1
II Test Setup	8
1 Data	8
2 Description of Apparatus	9
3 Test Procedure	10
4 Theoretical Assumptions	11
III Evaluation of Test Apparatus	13
1 Comparison of Preliminary Results with Theory	13
2 Review of Test Procedure	16
3 Modification of Test Apparatus	19
IV Test Results	22
V Conclusions	30
VI Recommendations	31
Appendix A Data Reduction	32
Appendix B Accuracy	55
Appendix C Modeling the Plate	56
Appendix D Insulation Requirements	97
References	103

LIST OF FIGURES

FIGURE	PAGE
1 Schematic of two-expander reverse Brayton cycle	1
2 Side view of sample heat-exchanger with six plates and five e-seal spacers	2
3 Top view of plate and e-seal spacer	3
4 E-seal geometry and hole misalignment	3
5 Configuration of test core	4
6 Assembled test section, e-seal spacer, and three plate types	5
7 Schematic of test apparatus (Dummy core in place)	9
8 Schematic of switch box operation	10
9 Comparison of predicted (punched plate) heat-transfer values with unmodified test results	15
10 Test section control volume	18
11 Comparison of measured and predicted heat leaks	20
12 Test section control volume	20
13a Photograph of punched and etched plate cross sections	23
13b Photograph of EBD plate cross section	24
14 Comparison of theoretical and actual friction factor data	25
15 Friction factor as a function of Reynolds number	26
16 Comparison of theoretical and actual heat-transfer characteristics	27
17 Effect of plate orientation on $N_{tu}/Plate$	28
18 Comparison of helium and air heat-transfer data	29
A1 E-seal dimensions	37
A2 Temp of air downstream from test section	54
C1 Model of staggered hole pattern	56
C2 Two pass heat exchanger	57
C3 Model of circular fin (High pressure flow path)	58
C4 Fin temperature properties	59

FIGURE		PAGE
C5	Model of a single hole	65
C6	Model of two holes	67
C7	Model of a sixth of a hole	69
C8	Plot of effective thermal conductivity ratio vs plate open area ratio	71
C9	Plot of pressure drop across one plate	72
D1	Schematic of test section	97
D2	Plot of heat leak rate vs insulation thickness (steady state analysis)	98
D3	Model of the insulated test section	99
D4	Transient analysis of heat loss with an infinite thickness of insulation	102

LIST OF TABLES

<u>TABLE</u>	<u>Title</u>	<u>PAGE</u>
1	Comparison of calculated and measured time to the maximum cooling rate	14
2	Comparison of actual and predicted apparent heat leak and time to maximum slope	21
A1	Friction factor data - punched and etched Plates (40 Plates/Core)	41-42
A2	Friction factor data - ERD plates	43-47
A3	Heat-transfer data - punched and etched plates (40 plates/core)	48-49
A4	Heat-transfer data - ERD plates	50-52
A5	Heat-transfer data - punched plate tested with air; original apparatus	53
B1	Maximum uncertainty of physical constants and measurements	55
C1	Theoretical friction factor for punched and etched plates	82
C2	Theoretical friction factor for ERD plates 20% open area	83-84
C3	N_{tu} /plate vs hole Reynolds number for the punched and etched plates	92
C4	Theoretical N_{tu} /plate assuming a parabolic velocity profile	93-96
D1	Comparison of different insulation requirements	100

SECTION I

INTRODUCTION

This report discusses testing and analysis Arthur D Little, Inc (ADL) conducted under the Rotary Reciprocating Refrigerator (RCUBE) Development Program [1]. The RCUBE cooler operates on a reverse-Brayton cycle to provide cooling at 60 K and 12 K. A schematic of the cycle is shown in Figure 1.

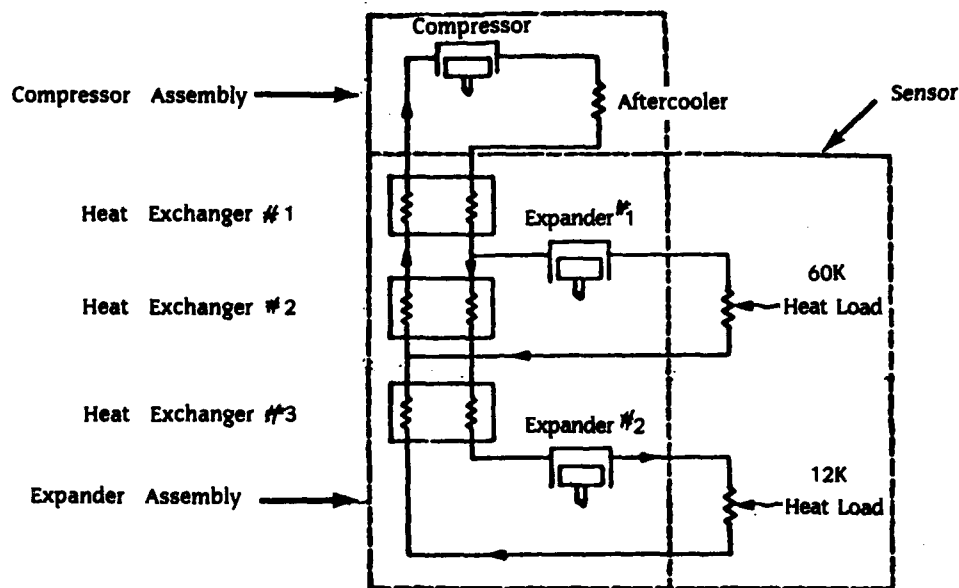


Figure 1. Schematic of two-expander reverse-Brayton cycle

The counterflow heat exchangers are vital cooler components -- typically each is required to have an effectiveness on the order of 0.98. Because of the large required effectiveness, the heat exchangers make up a significant portion of the cooler mass and volume. In order to reduce heat exchanger mass and volume, compact heat exchangers composed of perforated plates separated by G-10 spacers were developed. Unfortunately, the organic materials in the heat exchangers can outgas and contaminate the working fluid which reduces system life.

Since system life is a primary concern, an effort was undertaken to develop all-metal compact heat exchangers to replace the PCUBE heat exchangers which contained organic materials. The heat exchangers would be composed of copper perforated plates separated by stainless steel e-seal spacers. They would still be a two-pass counterflow design with the high pressure stream in the circular center section and the low pressure stream in the outer annular section (see Figures 2 and 3).

Note that the e-seal spacer has two functions. It both separates the two flow paths, and inhibits longitudinal conduction between adjacent plates. Because of the e-seal geometry, the physical plate separation is 0.087" while the conduction path length is 0.156" (see Figure 4).

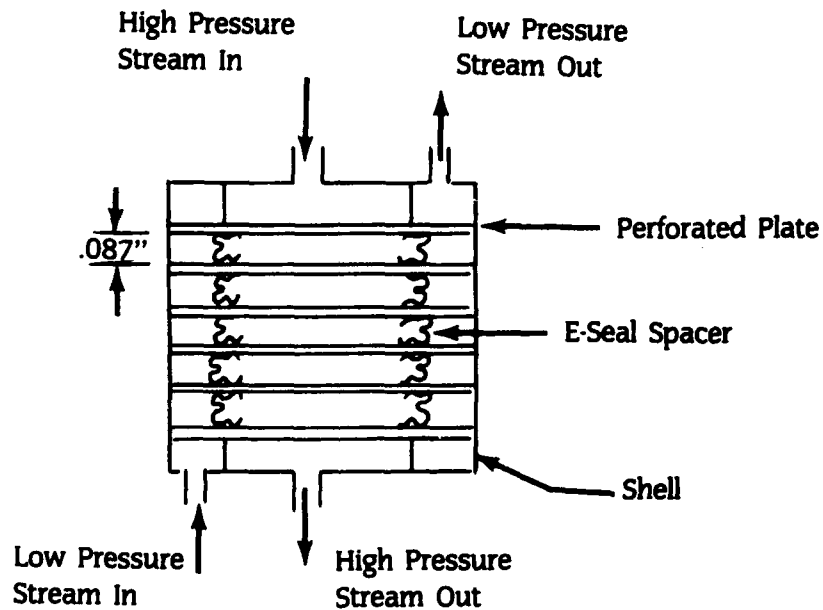


Figure 2. Side view of sample heat-exchanger with six plates and five e-seal spacers

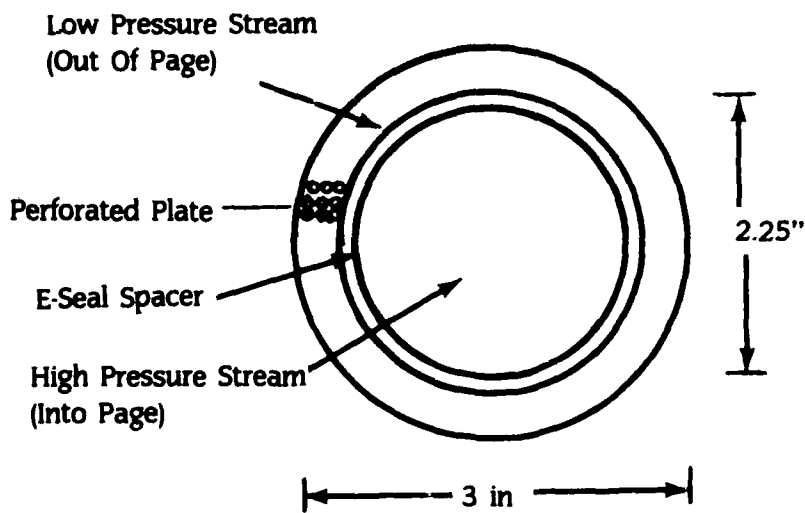


Figure 3. Top view of plate and e-seal spacer

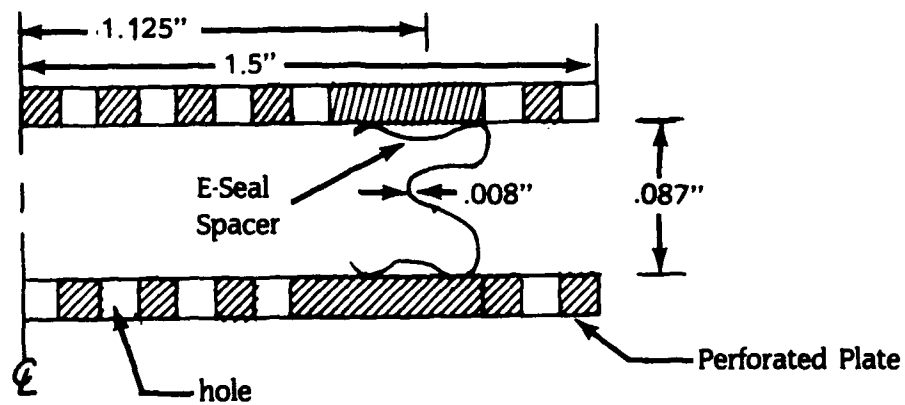


Figure 4. E-seal geometry and hole misalignment

Although the all-metal heat exchanger reduces contamination and therefore increases system life, it also results in a larger heat exchanger for a given effectiveness because it doesn't provide as much thermal isolation between the plates. Because system life is considered so important, the increase in system mass and volume is acceptable.

RCUBE system requirements dictate the minimum heat exchanger effectiveness and the maximum acceptable pressure drop across the heat exchangers. In order to design the heat exchangers, heat-transfer and pressure drop data had to be gathered for various plate geometries and flow conditions. The required effectiveness of the balanced, counterflow heat exchangers dictates the number of heat-transfer units (N_{tu}) for the entire heat exchanger. Consequently, N_{tu}/plate was chosen to compare the heat-transfer characteristics of various plate geometries. The friction factor was chosen to compare the pressure drop characteristics. Knowing the N_{tu}/plate and friction factor, the number of plates needed to achieve the required effectiveness and the associated heat exchanger pressure drop can be determined.

Next, test methods to determine N_{tu}/plate and friction factor were chosen. An isothermal pressure drop test was used to find friction factors while the single-blow transient test method [2] was used to gather heat-transfer data.

The single-blow transient test method allows a core of plates separated by e-seals to be tested using only one flow path (see Figure 5). The room temperature core is placed into a heated air flow and the air temperature downstream from the core is recorded until a steady state is reached. The core N_{tu} can be determined from the maximum slope of the time-temperature plot and the longitudinal heat conduction in the core.

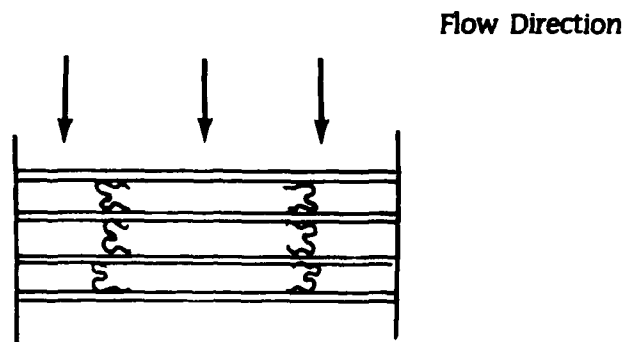


Figure 5. Configuration of test core

Since each plate in the core is isothermal at any given time during this test the N_{tu}/plate data reported is for 100% fin effectiveness. In order to use the data to design actual counterflow heat exchangers, the fin effectiveness must be considered (see Appendix C).

Eleven different plate geometries were tested and compared. The plate geometries that provided the best heat transfer and friction factors were identified. All the perforated plate test sections had 3" diameter copper plates separated by stainless steel e-seal spacers and were designed for a helium working fluid. Two test sections had plates with etched holes (9% and 24.5% open area), one had plates with punched holes (23.6% open area), and eight had plates manufactured using electron beam drilling (20% open area).

Originally the punched and etched plates were tested and the testing indicated that plates with smaller hole diameter to plate thickness (d/t) ratio had better heat-transfer characteristics. Consequently, ADL searched for a manufacturing method which could produce plates with smaller d/t ratios. They found the electron beam drilling process, so eight more cores ($0.154 \leq d/t \leq 0.750$) were manufactured and tested. The three original test cores had 40 plates separated by 39 e-seals. As thicker plates were manufactured, the cores had to have fewer plates to fit in the switching box -- the last 8 cores had 24 to 32 plates. Figure 6 shows an assembled test section, an e-seal spacer, and the three original plates.

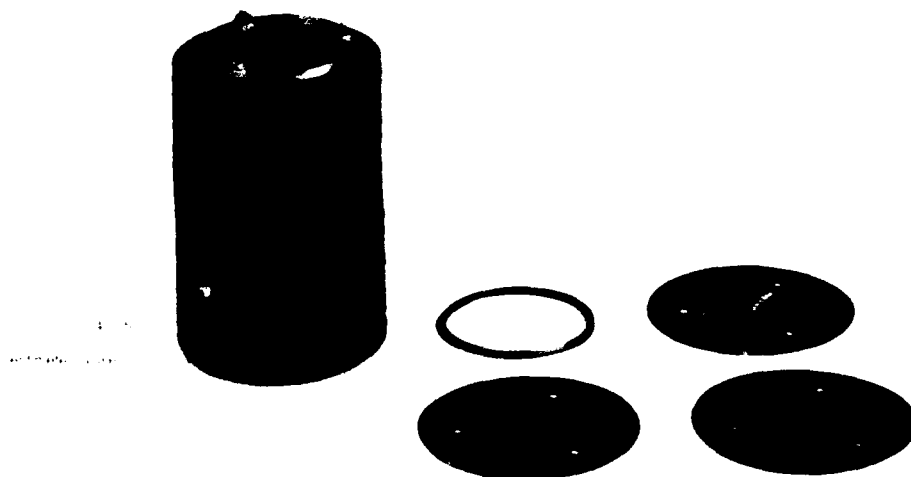


Figure 6. Assembled test section, e-seal spacer, and three plate types

Throughout the tests, the holes in the test cores were misaligned (see Figure 4). If the distance between the plates is small enough the alignment or misalignment of the holes is expected to affect both heat-transfer and pressure drop characteristics. Misaligning the holes is expected to enhance heat transfer while increasing pressure drop and aligning the holes is expected to minimize pressure drop at the expense of heat transfer. There is an indication [1] that if the ratio of plate separation to plate thickness is greater than one, the plates won't be influenced by adjacent plates. The ratio of plate separation to plate thickness ranged from 4.70 to 1.34 in the test cores. Consequently, the hole misalignment shouldn't affect the pressure drop through the cores. Furthermore, as long as total exchanger pressure drop remains acceptably small, it's desirable to enhance heat transfer at the expense of pressure drop.

This report describes the test methods and apparatus used to evaluate and compare the plates. Evaluations, and resulting modifications, of the test method and apparatus are also discussed. Data gathered using the final method were considered accurate enough for design purposes and were compared to theoretical results.

Section II discusses the characteristics chosen to compare the test sections and specifies the measurements necessary to calculate the plate characteristics. Next, this section describes the test apparatus and procedure. Finally, the assumptions of the single blow transient-test and the test conditions that closely approximate these assumptions are presented.

Section III shows the poor agreement between the test and theoretical results. The review of the test procedure and the subsequent modifications of the test apparatus are then discussed. Next, Section III verifies the accuracy of results obtained using the modified test apparatus. Section IV then presents the results. Sections V and VI cover conclusions and recommendations.

Appendix A presents the equations used to perform data reduction. The data, including a time-temperature trace from the modified apparatus and results are presented here and Appendix B describes the accuracy of the results.

The theoretical equations used to check the experimental data are derived in Appendix C. Appendix D compares the steady state and transient analysis to determine the insulation requirements.

The theory behind the single-blow transient test method is clearly presented by Pucci et al [2].

This report is based on a summary report [1] documenting tests performed by Mr Richard Hubbell. The tests were conducted at ADL under a contract to develop a two-stage rotary reciprocating refrigerator. Dr Fowle, a consultant to ADL, did the necessary analytical work to support the tests.

SECTION II

TEST SETUP

1. DATA

Since the objective of the tests was to compare test sections composed of different plates, a method of comparison had to be chosen. Since the number of heat-transfer units (N_{tu}) per plate will dictate the size of the heat exchanger for any required heat exchanger effectiveness, the N_{tu} /plate was selected to compare heat-transfer data. The friction factor (f) was selected for the pressure drop comparison and data were gathered for Reynolds numbers ranging from 4 to 666. The Reynolds number used for all calculations (hole Reynolds number) was calculated using a hole diameter as the representative length, and the mass flow rate was based on the minimum free flow area. The following properties were measured and used to calculate N_{tu} and f : the mass flow rate, the pressure drop across the test section, the temperature upstream and downstream from the test section as a function of time.

The N_{tu} is a function of the longitudinal heat conduction (thermal conduction in the solid, parallel to the flow direction) and the maximum slope of the temperature downstream from the test section vs time plot. The relationship between the longitudinal heat conduction, the maximum rate of change of temperature with time and the N_{tu} is presented in tabular and graphic form by Pucci [2]. Note that the Colburn modulus can be calculated given the heat-transfer number (N_{tu}), the Prandtl number (N_{pr}), and the plate geometry (A_c/A) using the following relationship:

$$j = N_{tu} (A_c/A) N_{pr}^{2/3} \quad (1)$$

where

j = Colburn modulus.

A_c = Minimum free flow area.

A = Total heat-transfer surface area.

N_{tu} = Number of heat-transfer units.

N_{Pr} = Prandtl number.

The friction factor per plate can be calculated given the mass flow rate and pressure drop across the test section during steady state operation.

$$f = \frac{D_h \Delta P \rho A_c^2 g_c}{2 n t \dot{m}^2} \quad (2)$$

where

f = Friction factor.

D_h = Hydraulic diameter.

ΔP = Pressure change across the test section.

ρ = Density of working fluid.

A_c = Minimum free flow area.

n = Number of plates.

t = Plate thickness.

\dot{m} = Mass flow rate.

g_c = Proportionality factor in Newton's second law.

$\frac{D_h A_c^2}{2 n t}$ is a physical property of the test section, and the temperature, pressure change, and volumetric flow rate were measured.

2. DESCRIPTION OF APPARATUS

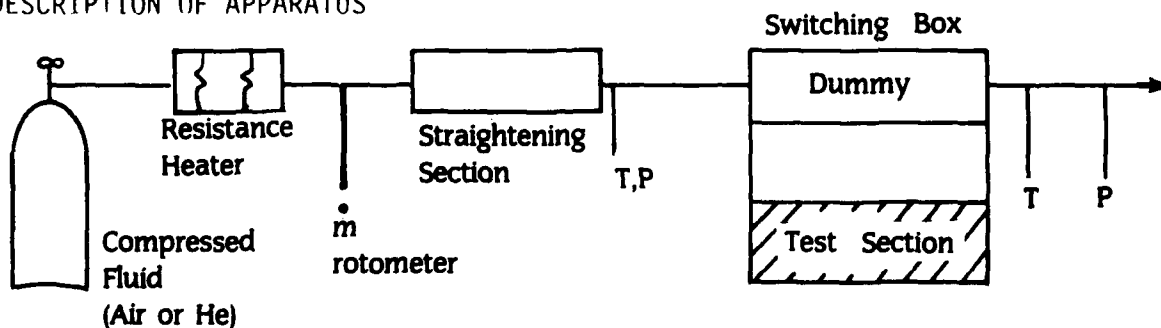


Figure 7. Schematic of test apparatus (dummy core in place)

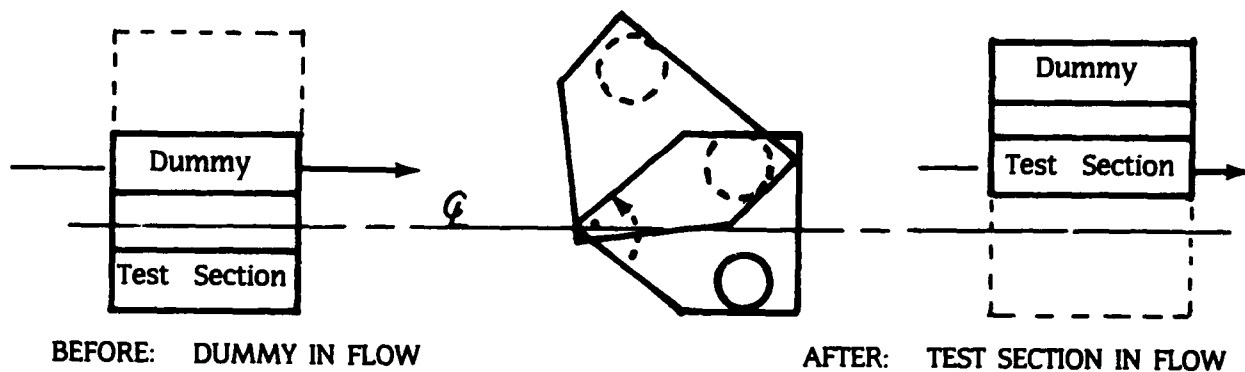


Figure 8. Schematic of switch box operation

The test apparatus (Figure 7) consists of a source of compressed air (or helium), a resistance heater followed by a flow straightening section and the test section. The test section is in a switching box (Figure 8) which allows it to be moved quickly into the stream of heated fluid. When the test section is not in the system, a dummy core, which causes the same pressure drop as the test section, is in place. Temperature and pressure readings are taken downstream from the straightening section, and the volumetric flow rate is measured upstream from the straightening section using a rotometer. The outlet temperature is measured after the switching box, and the outlet pressure tap is far enough downstream from the test section (~ 3 in) to allow for pressure recovery.

3. TEST PROCEDURE

The test procedure used to collect the data follows:

a. Number of Heat-Transfer Units (N_{tu})

(1) Establish a uniform temperature in the test core by blowing room-temperature compressed air, or helium, through the test apparatus with the test section in place. A uniform temperature ($\pm 0.1^\circ\text{F}$) is necessary through the entire test core volume to ensure repeatable results.

(2) Move the dummy section into the flow to allow the fluid to bypass the test section.

(3) Use the resistance heater to increase the fluid temperature about 20°F.

(4) Maintain the heated airflow until all the apparatus components reach a stable temperature. The time-temperature plot should vary less than 1.0°F/hr once this steady-state condition is achieved.

(5) Next, move the room-temperature test section into the hot air stream, and record the air temperature leaving the test section as a function of time. The pressure drop across the test section and the dummy section must be within 0.1" H₂O of each other to maintain a constant flow rate through the apparatus before and after the test section is moved into the stream.

(6) Repeat the procedure for various mass flow rates.

b. Friction Factor (f)

Record the pressure drop across the test section for steady-state, room-temperature fluid as a function of the flow rate.

4. THEORETICAL ASSUMPTIONS

The transient-test technique is based on assumptions which the test method and apparatus must insure. The assumptions and the test conditions that closely approximate each assumption follow:

a. The fluid temperature and velocity profiles are uniform across the cross-sectional area of the test section. The flow straighteners insure a uniform velocity profile, and the time-temperature plot shows when a steady-state, uniform temperature is reached.

b. The fluid flow rate is steady. This is assured by keeping a large reservoir of fluid and insuring that the pressure drop is the same across the test and dummy sections.

c. Longitudinal heat conduction is minimal. This is a design characteristic of perforated-plate heat exchangers.

d. Heat conduction across the core holder is negligible. An insulated balsa wood holder, which has low thermal capacity and conductivity, meets this requirement.

e. The matrix (core) heat-transfer coefficient is independent of position and time. The plate construction is uniform, and heat-transfer and fluid flow effects are distributed uniformly through the core.

f. The thermal properties of the test fluid are independent of temperature. A 20°F temperature change assures that the properties do not change substantially. This condition was tested by comparing the $N_{tu}/plate$ for 20, 30, and 40°F changes in air. The results were within 4% of each other for the same Reynolds number.

g. The gas acts as a perfect gas. At ambient temperature and pressure (test conditions) air and helium can be considered perfect gases. Also, using air as a test gas to gather data on helium heat exchangers is appropriate because the Prandtl numbers of air and helium are very close ($N_{Pr}(air) = 0.72$, $N_{Pr}(He) = 0.68$).

h. The thermal capacity of the gas in the matrix is small compared to the thermal capacity of the matrix. A core of 24 - 40 plates was used for the test assuring good thermal capacity.

i. Heat conduction in the gas is negligible in the flow direction. The convective heat transfer is much greater than any gas conduction effects.

SECTION III
EVALUATION OF TEST APPARATUS

1. COMPARISON WITH THEORY

The N_{tu}/plate can be determined as a function of plate geometry and hole Reynolds number. The equations used to calculate the N_{tu}/plate assume that

$$1 \leq N_{Re} \leq 1000$$

$$N_{Pr} = 0.7$$

and the section has a uniform wall temperature. Two laminar flow cases were considered. One case assumed a developing velocity profile in each hole and the other assumed a fully developed parabolic velocity profile. The results of the calculations in Appendix C follow.

FOR A DEVELOPING VELOCITY PROFILE

$$N_{tu}/\text{PLATE} = \frac{(1-\sigma)\sigma^{-0.232} (2.554+2.011 N_{Re}^{0.520} \sigma^{0.121})}{N_{Re}} + \frac{20.9 t/d}{N_{Re}} + \frac{0.417}{1+0.012[(d/t)N_{Re}]^{0.8}} \quad (3)$$

FOR A PARABOLIC VELOCITY PROFILE

$$N_{tu}/\text{PLATE} = \frac{(1-\sigma)\sigma^{-0.232} (2.554+2.011 N_{Re}^{0.52} \sigma^{0.121})}{N_{Re}} + \frac{20.9 t/d}{N_{Re}} + \frac{0.269}{1+0.032[(d/t)N_{Re}]^{0.667}} \quad (4)$$

where

N_{tu} = Heat-transfer number.

σ = Ratio of plate open area to frontal area.

t = Plate thickness.

d = Hole diameter.

N_{Re} = Hole Reynolds number.

Comparing the predicted values with the test results (Figure 9) showed that the predicted $N_{t,u}/\text{plate}$ are 2.3 to 4.7 times the test results. The actual and predicted times to maximum slope of the temperature vs time curve were also compared. The time to maximum slope (θ^*) is based on the mass flow rate and the fluid and heat exchanger properties.

$$\theta^* = \frac{m_m c_m}{\dot{m} c_p(\text{air})} \quad (5)$$

Where:

- \dot{m} = Mass flow rate of the fluid.
- m_m = Mass of plates.
- c_m = Specific heat of plates.
- $c_{p,air}$ = Specific heat of air (or helium).

Table 1 compares the calculated and measured time to maximum slope for runs 3 and 5.

RUN	θ^* (sec)	
	ACTUAL	PREDICTED
3	169	151
5	87.5	74.1

Table 1. Comparison of calculated and measured time to the maximum cooling rate

The actual values were read from the time temperature traces. The difference in the values indicates a fluid loss; however, it is very difficult to determine the time to maximum slope accurately from the traces.

Since there were large differences between the actual and predicted values of both the $N_{t,u}/\text{plate}$ and time to maximum slope, the test method and apparatus was suspect.

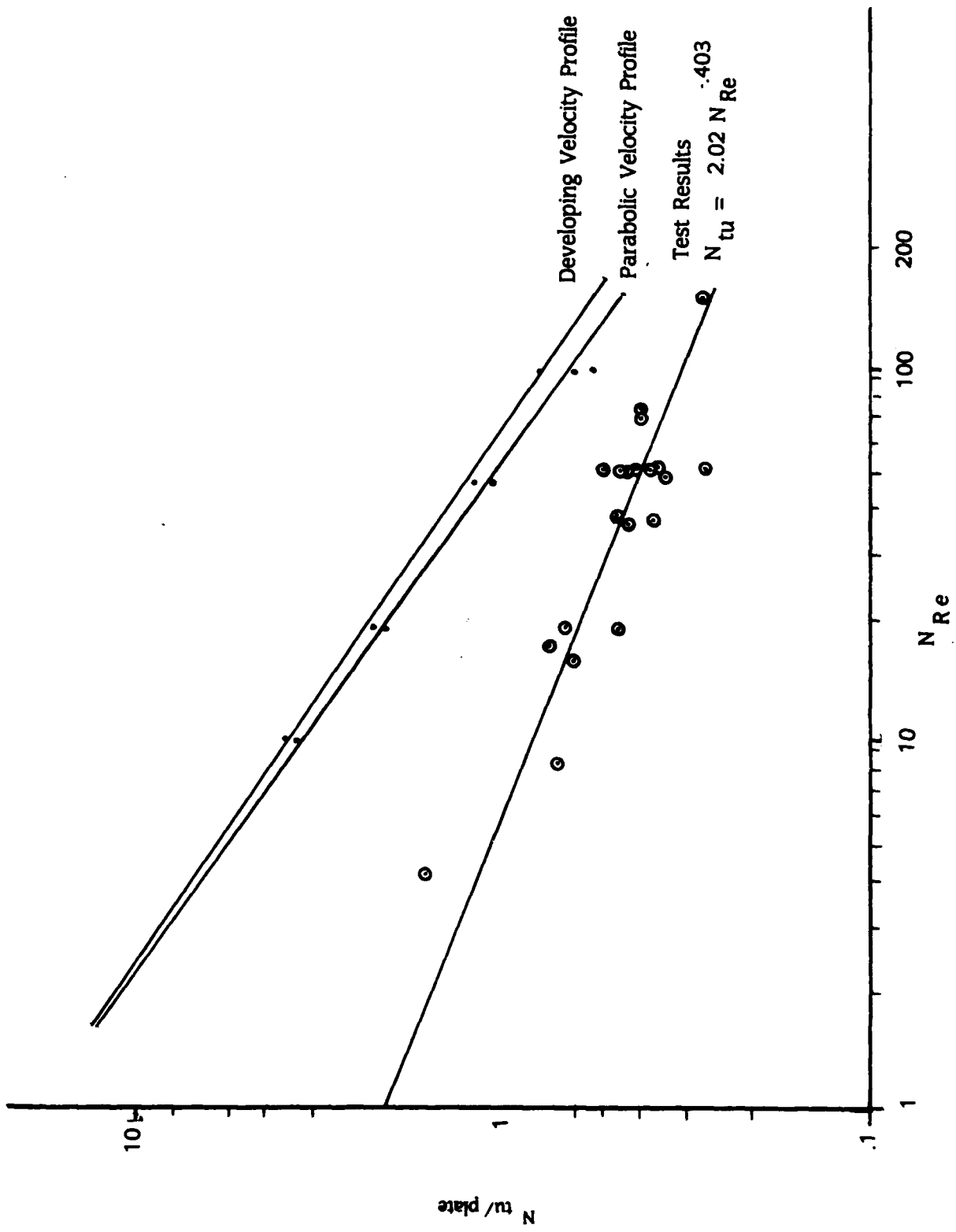


Figure 9. Comparison of predicted (punched plate) heat-transfer values with unmodified test results

2. REVIEW OF TEST PROCEDURE

Because of the discrepancy between predicted and measured values of $N_{tu}/plate$ vs N_{Re} and time to maximum slope, the test procedure was reviewed. The following aspects of the test were checked:

ASSUMPTIONS. Were the assumptions used to model the heat exchanger and predict the results met during the test?

INSTRUMENTATION. Was the instrumentation accurate enough to provide reliable data?

CALCULATIONS. Were the methods and calculations used to manipulate the data correct?

The instrumentation and calculations were fine; however, there was a large apparent heat leak that could have been due to either heat leaks, fluid leaks, or some combination of the two. The test apparatus model assumed that mass flow remained constant (no flow leakage) and that heat conduction across the core holder is negligible (no heat leakage). The assumptions upon which the transient-test technique is based were not met.

a. Heat Leaks

A heat leak was suspected when a temperature difference was noticed across the core once the system reached steady state. The instrumentation was checked -- it provided accurate sensing. The apparent heat leak was then estimated based on the following core information:

$T_i = 98^\circ\text{F}$	= Inlet temperature.
$T_o = 95.3^\circ\text{F}$	= Outlet temperature.
$\Delta T = 20^\circ\text{F}$	= Initial temperature step applied to the core.
$\dot{m} = 0.22 \text{ lbm/min}$	= Mass flow rate.
$\Delta\theta = 340 \text{ s}$	= Time to reach steady state.

$$\begin{aligned}
 m_s &= 1.287 \text{ lbm} && = \text{Mass of plates.} \\
 c_s &= 0.09 \text{ BTU/lbm R} && = \text{Specific heat of plate.} \\
 c_p(\text{air}) &= 0.24 \text{ BTU/lbm R} && = \text{Specific heat of air.}
 \end{aligned}$$

If the temperature difference was due only to a heat leak, the heat loss rate (\dot{q}_l) can be found from the following relationship:

$$\begin{aligned}
 \dot{q}_l &= \dot{m} c_p(\text{air}) (T_i - T_o) \\
 &= (0.22 \text{ lbm/min}) (0.24 \text{ BTU/lbm R}) (98 - 95.3) \text{ F} (60 \text{ min/hr}) \\
 &= 8.55 \text{ BTU/hr}
 \end{aligned}$$

To find the percent heat leak, the rate of heat storage must be estimated. The heat absorbed by the heat exchanger from the start of the test to steady state (Q) is calculated using the following equation:

$$\begin{aligned}
 Q &= m_s c_s \Delta T \\
 &= (1.287 \text{ lbm}) (0.09 \text{ BTU/lbm R}) (20^\circ \text{F}) \\
 &= 2.316 \text{ BTU}
 \end{aligned}$$

The average rate of heat storage (\dot{q}_s) can now be approximated:

$$\begin{aligned}
 \dot{q}_s &= \frac{Q}{\Delta \theta} = \frac{2.316 \text{ BTU}}{340 \text{ s}} (3600 \text{ s/hr}) \\
 &= 24.52 \text{ BTU/hr}
 \end{aligned}$$

The resulting apparent heat loss rate ($\dot{q}_l = 8.55 \text{ BTU/hr}$) is 35% of the heat storage rate ($\dot{q}_s = 24.52 \text{ BTU/hr}$) -- this is an unacceptable loss.

h. Fluid Leaks

The apparent heat leak may be partially due to fluid leaks. A reasonable estimate of the heat leak is 4.5 BTU/hr. If the heat leak was actually only 4.5 BTU/hr, the fluid leak can be estimated by performing an energy balance on the system.

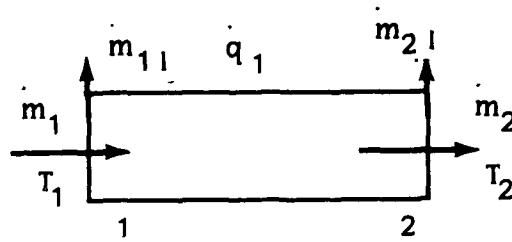


Figure 10. Test section control volume

The fluid loss at Section 1 is the critical loss; any loss at Section 2 should not significantly affect the test.

$$\int q_1 dt = \int \frac{dE}{dt} dt + \int (\dot{m}_2 + \dot{m}_{2l}) c_p T_2 dt + \int (\dot{m}_{1l} + \dot{m}_1) c_p T_1 dt$$

where

\dot{m}_1 = Mass flow into test section.

\dot{m}_{1l} = Mass flow leaking out of test section at the entrance.

\dot{m}_2 = Mass flow out of the test section.

\dot{m}_{2l} = Mass flow leaking out of the test section at the exit.

t = Time.

E = Internal energy.

$$\Delta \dot{m}_1 = \frac{\dot{m}_{1l}}{\dot{m}_1} (100\%) = \text{Percent fluid loss.}$$

The following relationship results from the continuity equation:

$$\dot{m}_2 + \dot{m}_{21} = \dot{m}_1 - \dot{m}_{11}$$

Now, assuming all the flows are constant, for the steady-state condition the percent fluid loss can be found directly from the following relationship:

$$\begin{aligned} \Delta \dot{m}_{11} &= 1 - \frac{\dot{q}_1}{\dot{m}_1 c_p (T_1 - T_2)} (100\%) \\ &= 1 - \frac{4.5 \text{ BTU/hr}}{(0.22 \text{ lbm/min}) (0.24 \text{ BTU/lbm R})(2.7\text{F}) 60 \text{ min}} \text{ hr} \\ &= 47\% \end{aligned}$$

The calculations indicated the need to modify the apparatus to reduce both heat and fluid leaks.

3. MODIFICATION OF TEST APPARATUS

The test apparatus was modified using a seal tight design to reduce fluid leaks and more effective insulation to reduce heat leaks. The transient behavior of the insulation, not the steady state behavior, determined how much insulation was needed. Figure 8 compares the estimated total heat loss vs time calculated using steady state and transient analysis. Measured values of the apparent heat leak are also presented. Runs 25 and 30 were performed using the modified apparatus. Before the modification, the discrepancy between the measured and predicted values (using both steady state and transient analysis) of the heat leak were large. After the modification the heat leak for long runs had decreased considerably and the measured and predicted values (using transient analysis) were much closer.

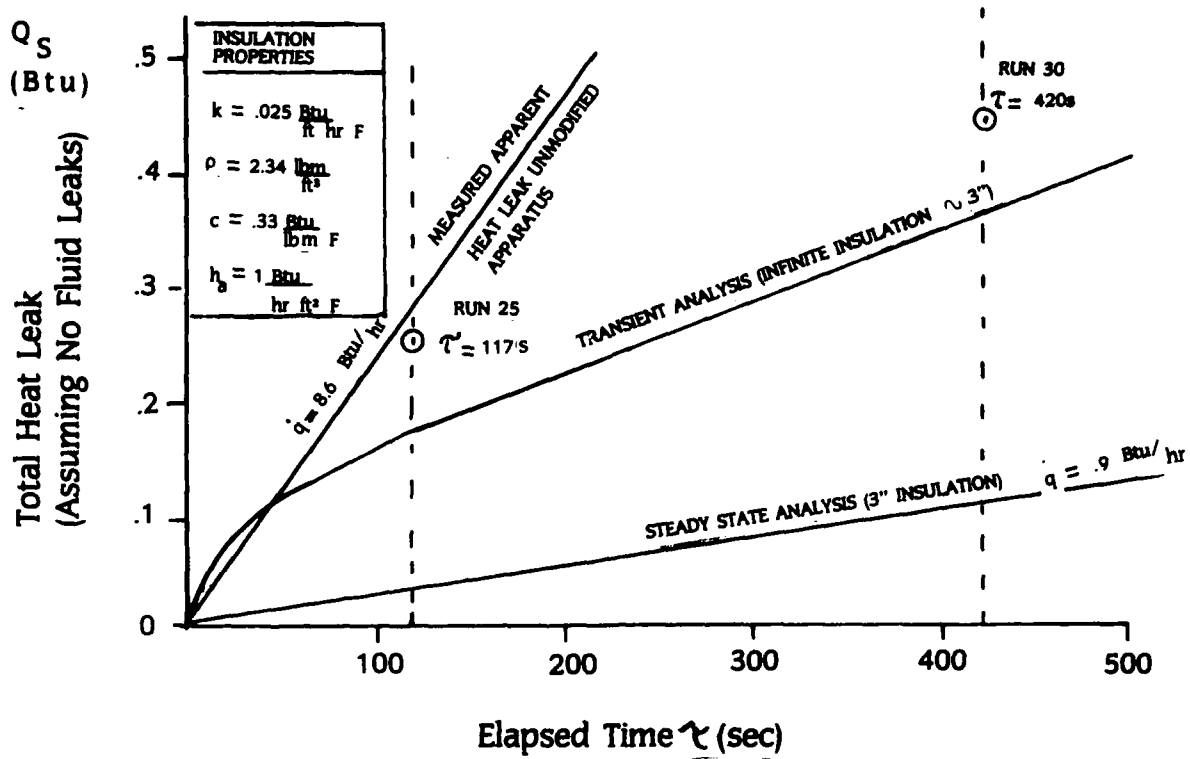


Figure 11. Comparison of measured and predicted heat leaks

The modified apparatus reduced heat and flow leaks, producing results accurate enough for design evaluations. The accuracy of the apparatus can be demonstrated by comparing the actual and theoretical apparent heat leaks and time to the maximum temperature slope for various runs.

The heat loss from the system was found using an energy balance assuming no fluid leakage.

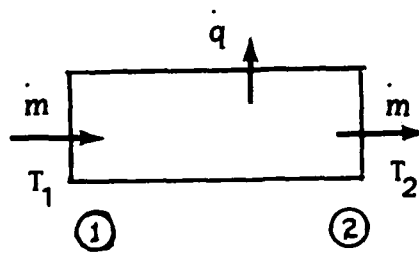


Figure 12. Test section control volume

$$\begin{aligned}
 Q_{\text{loss}} &= \int_0^{\tau} \dot{Q} dt = \int_0^{\tau} \frac{dE}{dt} dt + \int_0^{\tau} \dot{m} c_p T_2 dt - \int_0^{\tau} \dot{m} c_p T_1 dt \\
 &= -m_m c_m (t_f - t_i) + \dot{m} c_p \int_0^{\tau} (T_1 - T_2) dt
 \end{aligned}$$

where

m_m = Mass of core.

c_m = Specific heat of core.

t_f = Temperature of core at final steady state.

t_i = Temperature of core before heating.

$\int_0^{\tau} (T_1 - T_2) dt$ = Area under the temperature vs time plot.

τ = Time for the run to reach steady state.

The test generates data to calculate the actual heat leak. The predicted heat loss for infinite insulation can be estimated using tabulated values of heat loss as a function of insulation properties and the time needed to reach the steady-state condition. The actual time to maximum slope can be read from the time-temperature plot and equation (5) generates the predicted time to maximum slope.

The results of the comparisons for test runs 25 and 30 are presented in Table 2. The runs show excellent agreement between the predicted and measured values and indicate minimal heat and fluid losses.

RIIN	τ (sec)	Q (BTU)		θ^* (sec)	
		Measured	Predicted	Measured	Predicted
25	117	0.25	0.17	38.0	38.9
30	420	0.45	0.35	293	298

Table 2. Comparison of actual and predicted apparent heat leak and time to maximum slope

SECTION IV

TEST RESULTS

The three heat exchanger core types (punched, etched, and electron beam drilled (EBD)) were tested four ways. The punched and EBD plates have a breakout caused by manufacturing (See Figure 13). Tests were run with the breakout facing both upstream and downstream. The orientation of the core affected the N_{tu}/plate but did not affect the friction factor. Since the etched plates do not have breakouts, orientation was not considered. The etched plates were tested with both helium and air to insure there was not a significant Prandtl number effect--there wasn't.

Figure 14 presents both the theoretical and measured friction factors as a function of hole Reynolds number. The theoretical results were calculated using equation (C44) and are presented in Tables C1 and C2. The theoretical results show that the friction factor decreases as the percent open area increases and as the hole diameter to plate thickness ratio decreases. The experimental results indicate that the friction factor is more sensitive to the hole diameter to plate thickness ratio than the percent open area. As the hole diameter to plate thickness ratio decreases, the friction factor also decreases.

Figure 15 shows that the friction factor data didn't depend on the test gas (air or helium) or the core orientation.

Figure 16 presents the theoretical and measured heat-transfer data. The theoretical results presented assume a parabolic velocity profile in the holes, were calculated using equations in appendix C, and are tabulated in Tables C3 and C4. The theoretical results indicate that N_{tu}/plate increases with decreasing d/t ratio. The experimental results indicate that for hole Reynolds numbers above 30, the N_{tu}/plate increases as d/t decreases. Also, the slope of the N_{tu}/plate vs N_{Re} decreases as d/t increases.

Figure 17 demonstrates the dependence of the heat-transfer data on plate orientation (or hole shape). Both the punched and EBD plates were oriented in the core with all the hole breakouts facing the same direction. When the core was

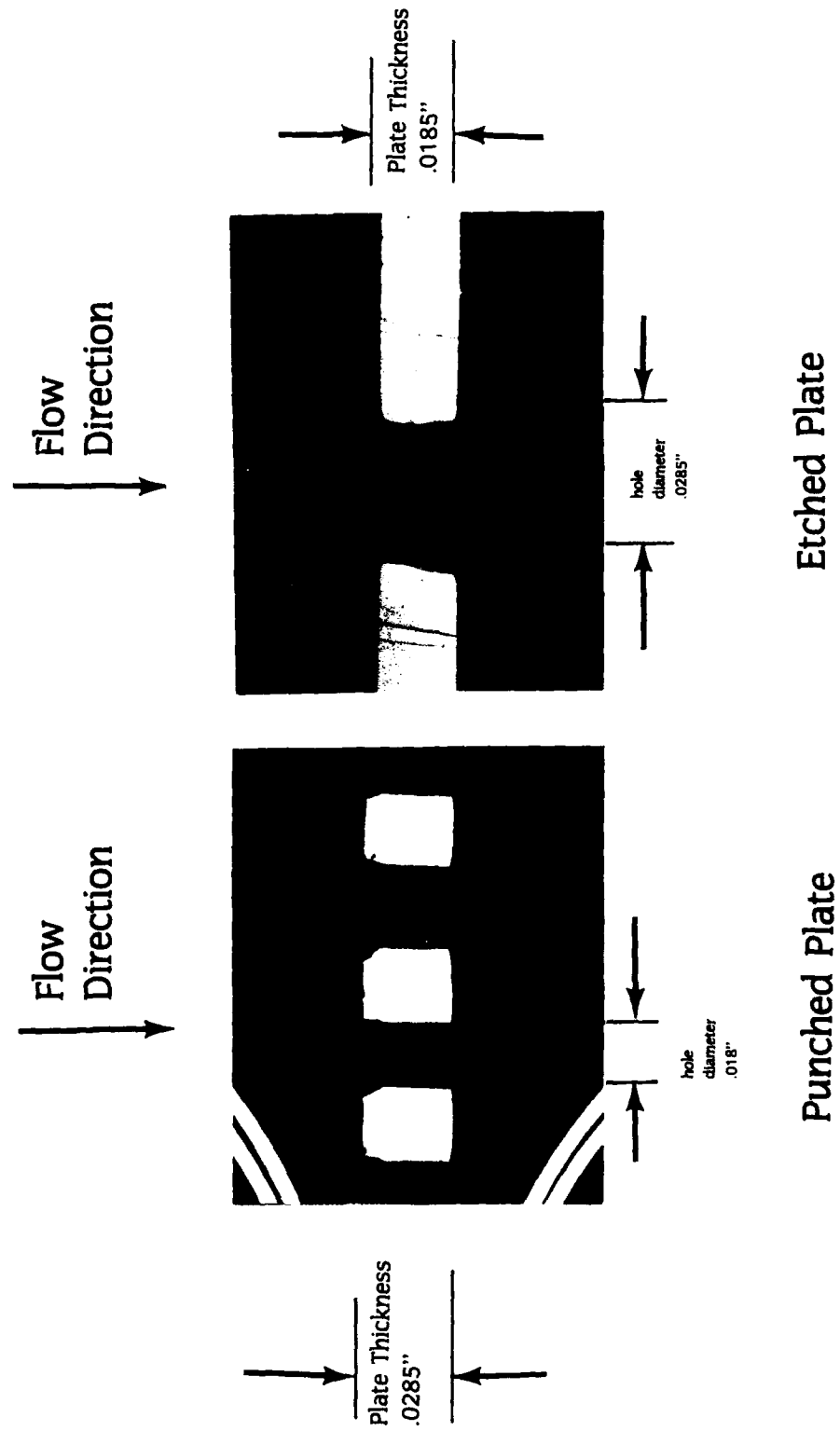


Figure 13a. Photograph of punched and etched plate cross section



Figure 13b. Photograph of EBD plate cross section ($t = .065''$, $d = .010''$)

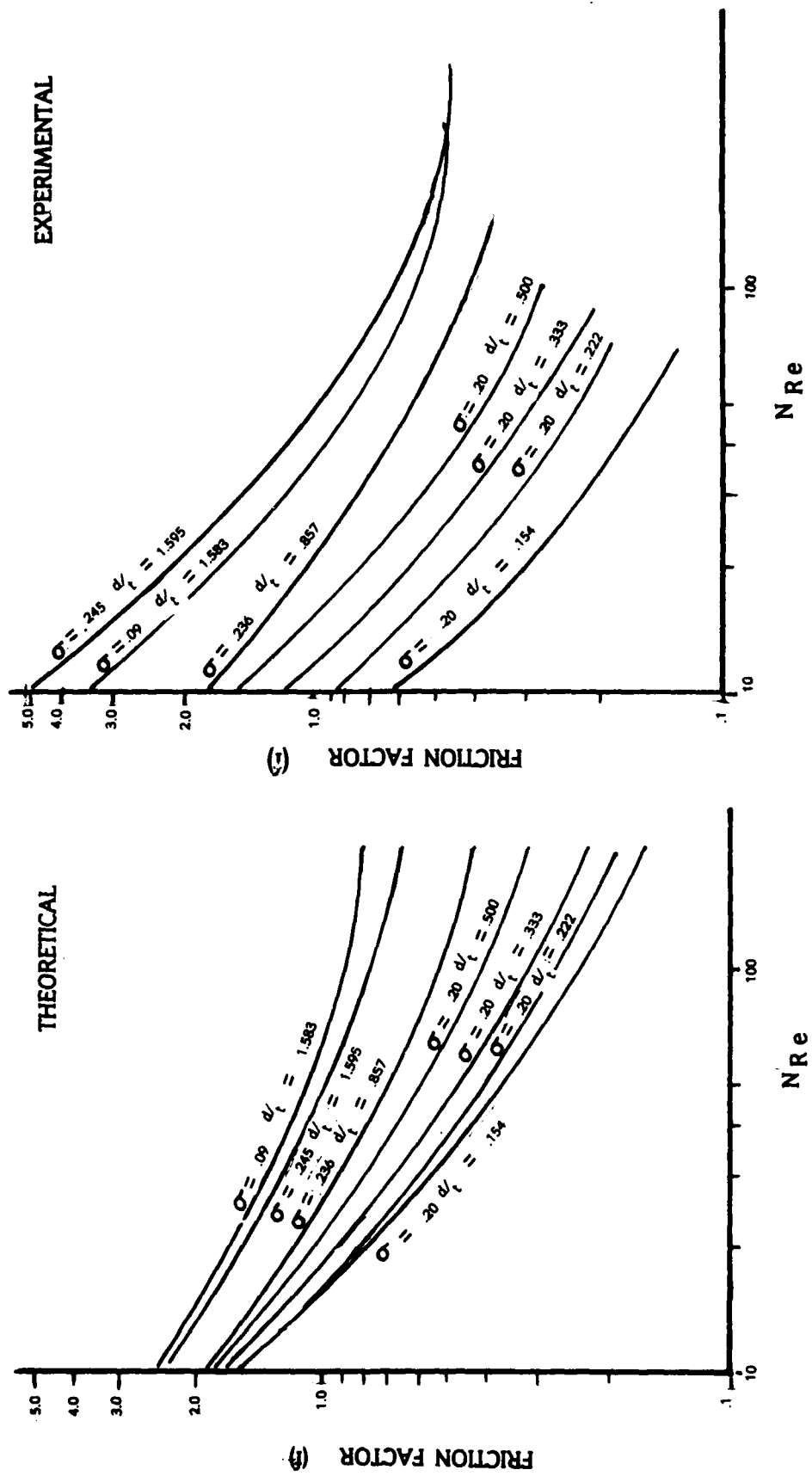


Figure 14. Comparison of theoretical and actual friction factor data

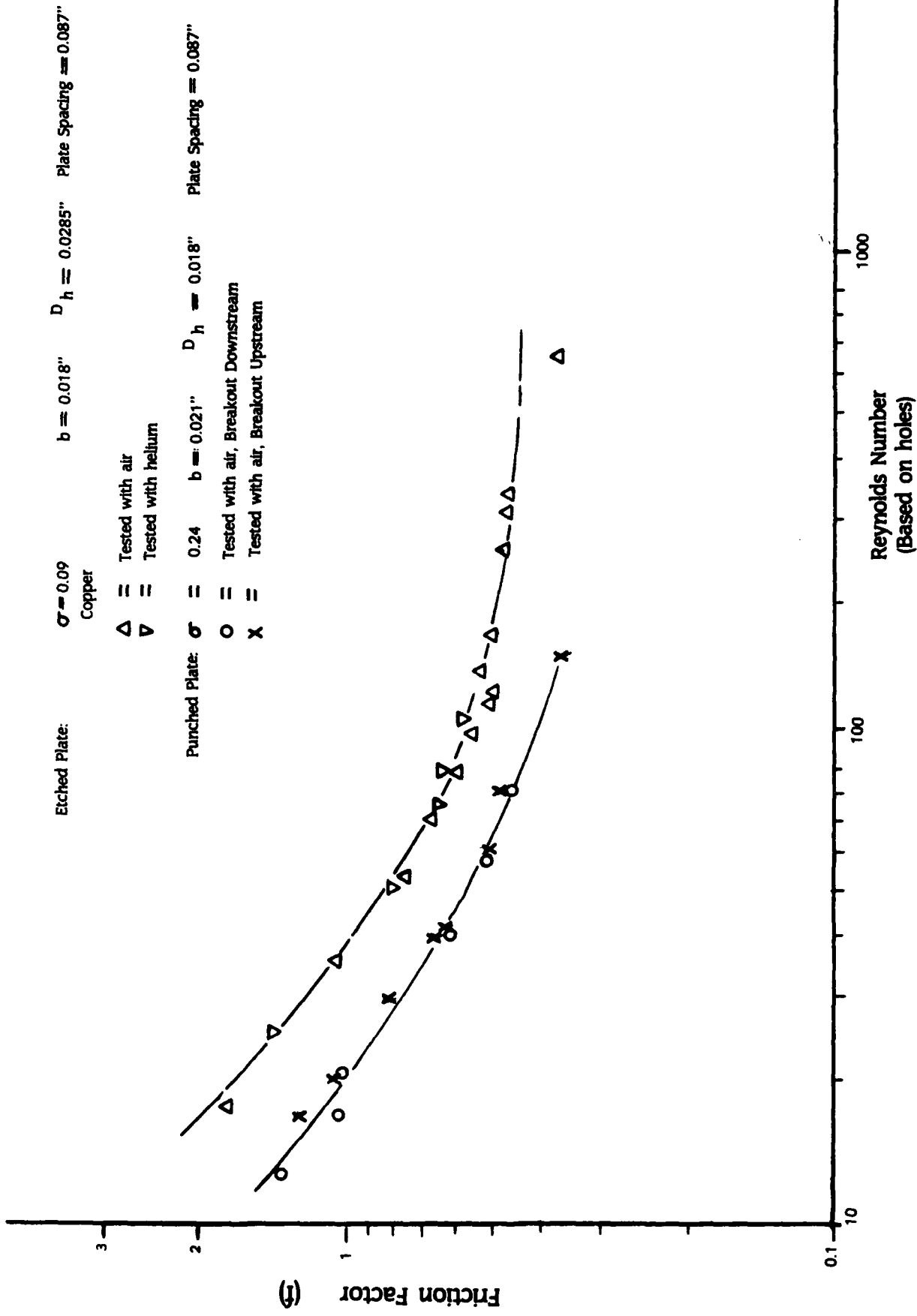


Figure 15. Friction factor as a function of Reynolds number

EXPERIMENTAL

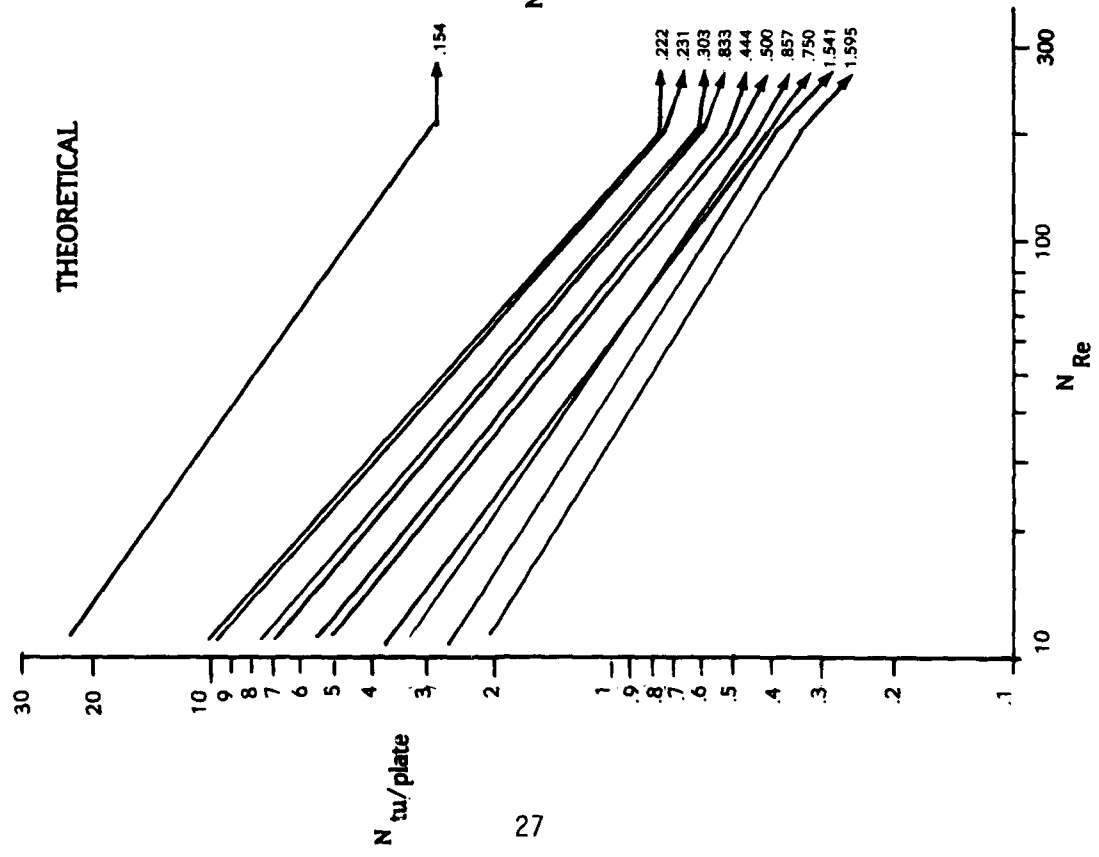
$$N_{tu/plate} = b N_{Re}^m$$

d/t	σ	b	m
.154	.20	.995	-.093
.222	.20	.939	-.168
.231	.20	1.66	-.291
.308	.20	1.98	-.313
.333	.20	2.03	-.313
.444	.20	3.23	-.435
.500	.20	2.52	-.428
.750	.20	3.36	-.477
.857	.236	3.60	-.501
1.541	.09	2.10	-.372
1.595	.245	4.13	-.594

THEORETICAL

$$N_{tu/plate} = b N_{Re}^m$$

d/t	σ	b	m
.154	.20	116.6	-.707
.222	.20	77.78	-.878
.231	.20	74.62	-.875
.308	.20	54.39	-.848
.333	.20	49.86	-.840
.444	.20	36.62	-.810
.500	.20	32.38	-.798
.750	.20	21.56	-.754
.857	.236	15.89	-.687
1.541	.09	11.02	-.634
1.595	.245	9.632	-.640



EXPERIMENTAL

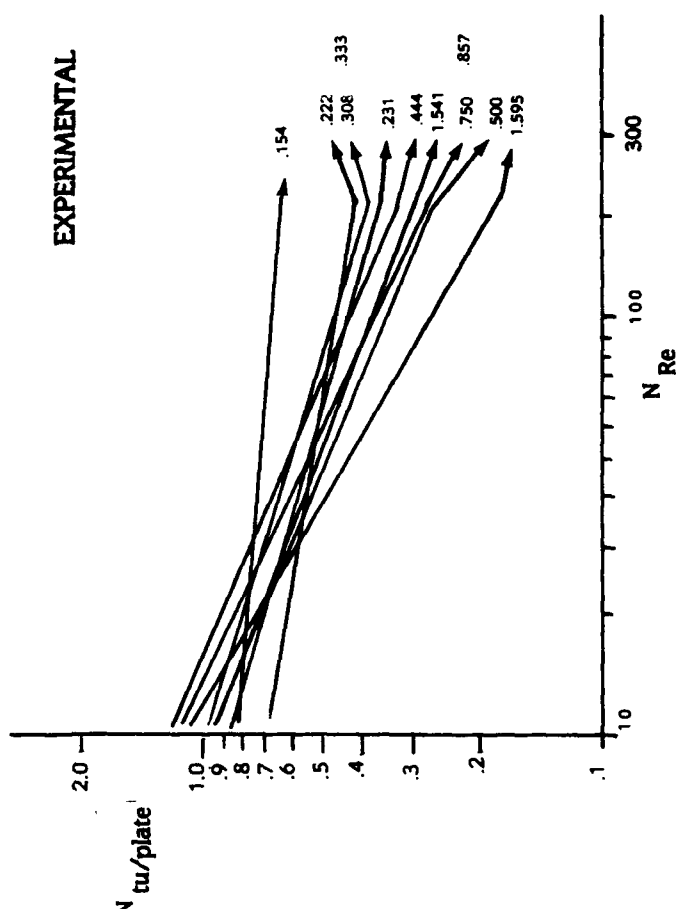


Figure 16. Comparison of theoretical and actual heat-transfer characteristics

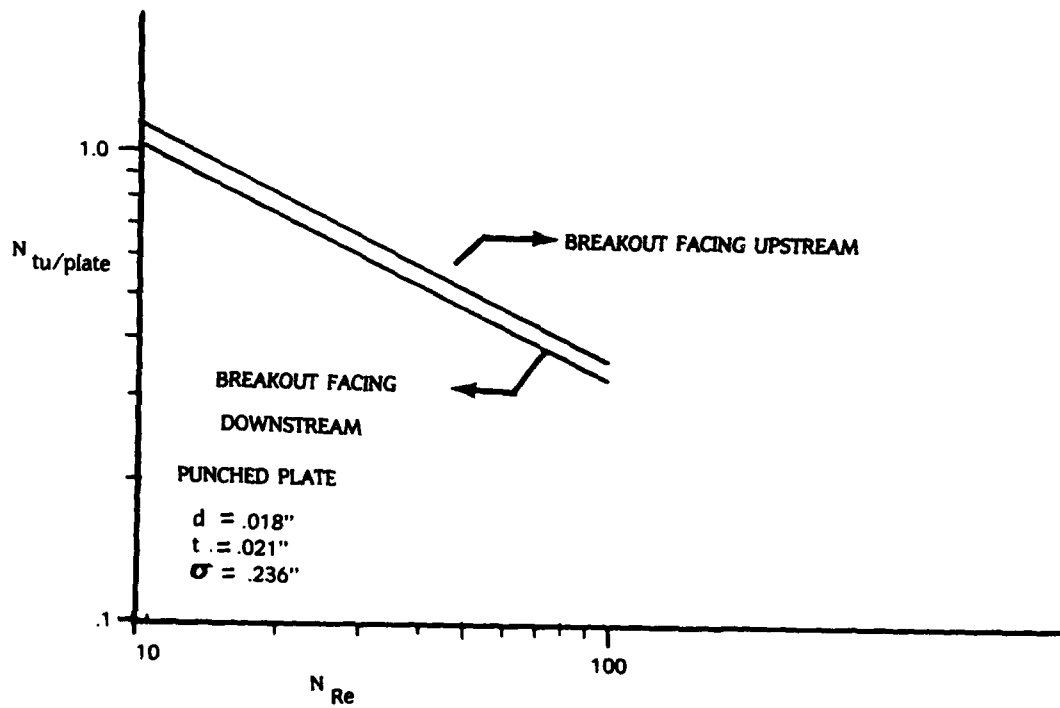
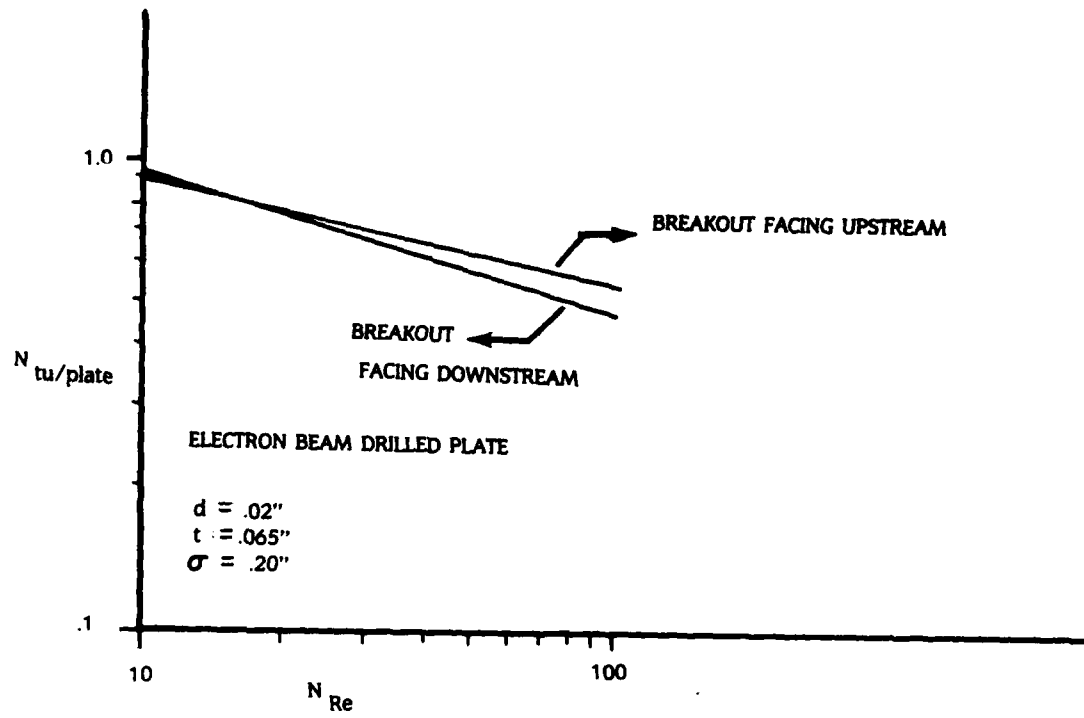


Figure 17. Effect of plate orientation on $N_{tu}/plate$

oriented so the fluid in the holes followed a converging path, the $N_{tu}/plate$ for a given N_{Re} was higher than for a core oriented so the fluid followed a diverging path. This small, but measurable, increase in $N_{tu}/plate$ is probably due to less flow separation in the holes.

The heat-transfer data didn't depend on the test gas (Figure 18).

Note that the theoretical heat-transfer predictions are not accurate. Both the predicted slope and intercepts are off resulting in predictions that are too high (by as much as a factor of 20 for low N_{Re} and low d/t). Also, the model failed to predict that larger d/t ratios result in larger drops in $N_{tu}/plate$ as N_{Re} increases. The discrepancies are probably due to uncertainty over actual fluid flow in the holes. Clearly hole shape affects the heat-transfer data and the model assumes cylindrical holes with no flow separation. Actually the holes are not cylindrical and there may be flow separation which accounts for the lower measured $N_{tu}/plate$ values.

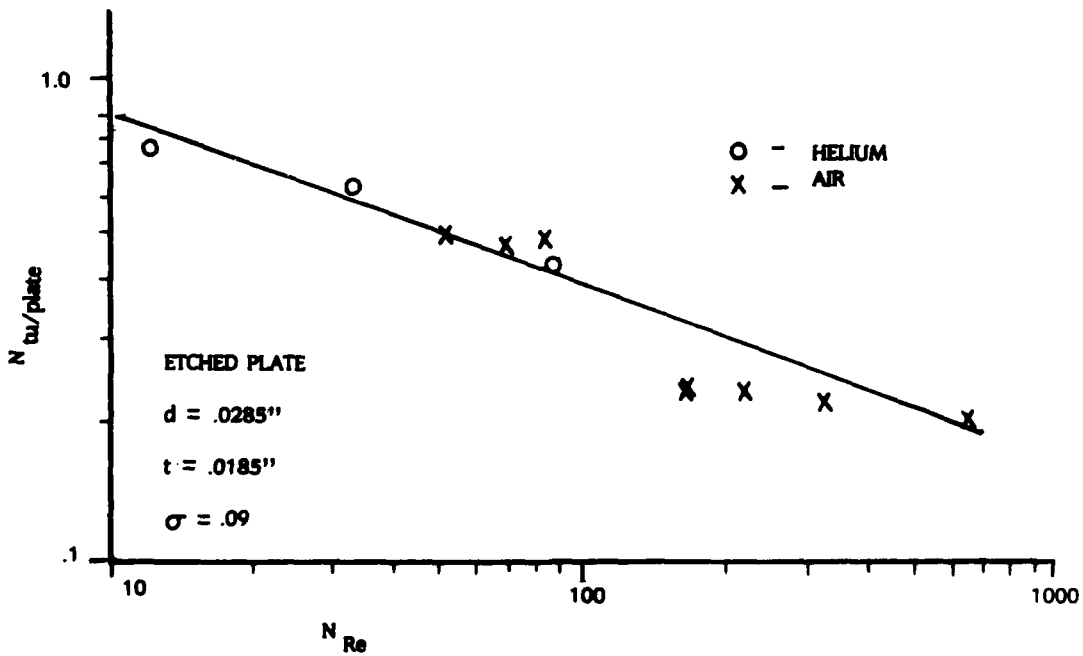


Figure 18. Comparison of helium and air heat-transfer data

SECTION V

CONCLUSIONS

1. The modified apparatus using the single blow transient test method to determine the heat-transfer characteristics of perforated-plate heat exchangers produces results accurate enough for design evaluations.
2. The transient test method is somewhat insensitive to heat leaks when used to determine the average heat-transfer characteristics of perforated-plate heat exchangers. The test technique is; however, very sensitive to heat leaks (and all assumptions) on an individual basis. If the assumptions aren't insured by the test method, the individual results aren't repeatable.
3. Transient behavior dictates the amount of insulation needed for the test section, not steady-state conditions.
4. Air can be used to test heat exchangers designed for helium systems.
5. Hole shape affects the heat-transfer characteristics. The increase in N_{tu}/plate when the punched and ERD plates were tested with the breakout facing upstream indicates that a converging-diverging hole may provide better heat-transfer characteristics.
6. Heat-transfer characteristics depend strongly on the hole diameter to plate thickness ratio. For hole Reynolds numbers greater than 30, the N_{tu}/plate increases as d/t decreases. Also, the N_{tu}/plate doesn't decrease as quickly with increasing N_{Re} for smaller d/t ratios.
7. The model used to determine the N_{tu}/plate doesn't completely describe the system. The correlation between the theoretical and experimental results is poor, but is better assuming a parabolic velocity profile instead of a developing velocity profile in the holes. The difference between the predicted and actual values is probably due to uncertainty over actual flow conditions in the holes.

SECTION VI

RECOMMENDATIONS

1. Further investigation should be conducted to determine the effect of hole shape on $N_{tu}/plate$. Also, manufacturing techniques should be investigated to find ways to manufacture plates with a smaller d/t ratio.
2. Use an analog to digital converter and a minicomputer to record the temperature downstream from the test section. This will reduce the possible error in reading the slope and will reduce the corresponding error in the $N_{tu}/plate$ vs hole Reynolds number from $\pm 6\%$ (low N_{Re}) or $\pm 3\%$ (higher N_{Re}) to less than $\pm 1\%$.

APPENDIX A - DATA REDUCTION

The test sections that were tested are shown in Figure 1. Temperature, pressure, volumetric flowrate, and the time-temperature history were recorded for each run. This data was reduced using the following method to calculate the Colburn modulus and friction factor vs hole Reynolds number. The calculations are presented in the following order: mass flow, hole Reynolds number, number of heat-transfer units, Colburn modulus, and friction factor.

1. MASS FLOW

Start with the definition of mass flow:

$$\begin{aligned}\dot{m} &= \rho A_c V & (A1) \\ &= V_f \dot{V} \\ &= V_f \sqrt{\rho^2}\end{aligned}$$

Assume: Perfect Gas

$$\begin{aligned}\rho &= \frac{P}{RT} \\ \dot{m} &= V_f \sqrt{\frac{\rho P}{RT}} \\ \dot{m} &= \frac{V_f}{\sqrt{R}} \sqrt{\frac{\rho P}{T}} & (A2)\end{aligned}$$

Where:

- V = Velocity of fluid entering test section.
 A_C = Open area of plate.
 \dot{m} = Mass flow rate.
 $V_f = VA_C$ = Volumetric flow rate.
 R = Gas constant.
 ρ = Density.
 P = Pressure.
 T = Temperature.

The volumetric flow rate is available as a percentage of a full-scale reading.

Let:

- G_F = Flow meter full-scale flow.
 S_R = Scale reading.
 $R_{Air} = 53.34 \frac{\text{ft lbf}}{\text{lbm R}}$
 $R_{He} = 386.0 \frac{\text{ft lbf}}{\text{lbm R}}$

$$\dot{m} = \frac{S_R (G_F)}{\sqrt{R}} \sqrt{\frac{\rho P}{T}}$$

$$\dot{m} = \frac{S_R [G_F (\text{ft}^3/\text{min})]}{\sqrt{53.34 \frac{\text{ft lbf}}{\text{lbm R}}}} \sqrt{\frac{\rho \left(\frac{\text{lbm}}{\text{ft}^3}\right) P \left(\frac{\text{lbf}}{\text{in}^2}\right)}{T (R)}} \left(\frac{12 \text{ in}}{\text{ft}}\right)$$

For air:

$$\dot{m} \text{ (lbm/min)} = 1.6444 S_R G_F \text{ (ft}^3\text{/min)} \sqrt{\frac{\rho \left(\frac{\text{lbm}}{\text{ft}^3}\right) P \left(\frac{\text{lb}_f}{\text{in}^2}\right)}{T \text{ (R)}}} \quad (\text{A3})$$

For helium:

$$\dot{m} \text{ (lbm/min)} = 0.611 S_R G_F \text{ (ft}^3\text{/min)} \sqrt{\frac{\rho \left(\frac{\text{lbm}}{\text{ft}^3}\right) P \left(\frac{\text{lb}_f}{\text{in}^2}\right)}{T \text{ (R)}}} \quad (\text{A4})$$

NOTE: Use upstream fluid properties.

2. HOLE REYNOLDS NUMBER

Again, start with the definition of the hole Reynolds number:

$$\begin{aligned} N_{Re} &= \frac{\rho V D_h}{\mu} \\ &= \frac{\dot{m} D_h}{A_c \mu} \end{aligned} \quad (\text{A5})$$

FROM THE DEFINITION OF A_c :

$$A_c = \frac{\sigma(\pi D^2)}{4}$$

$$= \sigma \pi \left(\frac{9}{4} \right) \text{ in}^2$$

$$N_{Re} = \frac{4\dot{m}D_h}{9\sigma\pi\mu}$$

$$= \frac{4\dot{m} (\text{lbm/min}) D_h (\text{in})}{\sigma\pi(9\text{in}^2) \mu \left(\frac{\text{lbm}}{\text{sec ft}} \right)} \quad \frac{\text{min}}{60\text{sec}} \quad \frac{12\text{in}}{\text{ft}}$$

$$N_{Re} = \frac{2.829 \times 10^{-2} \dot{m} (\text{lbm/min}) D_h (\text{in})}{\sigma \mu (\text{lbm/s ft})}$$

Where:

\dot{m} = Mass flow rate.

D_h = Hydraulic diameter of hole.

D = Plate diameter.

d = Hole diameter.

σ = Ratio of the plate open area to frontal area.

μ = Fluid viscosity.

The Reynolds number is based on the characteristics of one hole. Note that the hydraulic diameter of any cylindrical pipe is the pipe's diameter. Consequently, the equation for Reynolds number can be rewritten as follows.

$$N_{Re} = \frac{2.829 \times 10^{-2} \dot{m} (\text{lbm/min}) d (\text{in})}{\sigma \mu (\text{lbm/s ft})} \quad (\text{A6})$$

3. NUMBER OF HEAT-TRANSFER UNITS

Pucci [2] presents the N_{tu} as a function of the maximum slope and longitudinal conduction parameters both graphically (Figure 3[2]) and tabularly (Table 1[2]). To find the N_{tu} , the maximum slope and longitudinal conduction parameters must be calculated.

a. MAXIMUM SLOPE PARAMETER

The maximum slope parameter is defined as follows:

$$\text{MAX. SLOPE PAR} = \frac{dt_{f2}/d\theta \Big|_{\max}}{\frac{\dot{m} c_p \Delta t_{f1}}{M_s C_s}} \quad (\text{A7})$$

Where:

- $\frac{dt_{f2}}{d\theta} \Big|_{\max}$ = The maximum slope of the trace of outlet temperature vs time.
- Δt_{f1} = Step change imposed on inlet gas temperature.
- M_s = The mass of the heat-transfer core.
- C_s = The specific heat of the heat-transfer core.
- c_p = The specific heat of the fluid.
- \dot{m} = Mass flow rate of the fluid.

The mass of the core can be determined from the plate geometry and the number of plates.

$$M_s = \left(\frac{\pi D^2}{4} \right) (1-\sigma) t n p \quad (\text{A8})$$

where

- D = Plate diameter.
- α = Ratio of plate open area to frontal area.
- ρ = Density of plate.
- t = Plate thickness.
- n = number of plates in the core.

b. Longitudinal Conduction Parameter

The longitudinal conduction parameter is defined by the following ratio:

$$\lambda = \frac{\text{longitudinal heat transport by solid conduction}}{\text{heat transport to flowing gas}}$$

The longitudinal heat transport by solid conduction can be broken into two components: conduction in the e-seals and conduction in the shell.

$$\lambda = \frac{\frac{k_k A_k}{L_k} + \frac{k_{e\text{-seal}} A_{e\text{-seal}}}{L_{e\text{-seal}}}}{m c_p} \quad (\text{A9})$$

$$\begin{aligned} k_k &= 9 \text{ BTU/hr ft R} && \text{(stainless steel)} \\ A_k &= 0.015 \text{ in}^2 \\ L_k &= 4.2 \text{ in} \end{aligned}$$

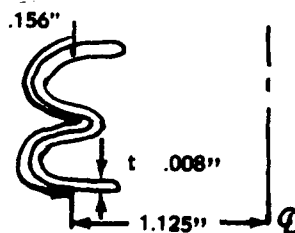


Figure A1. E-seal dimensions

$$\begin{aligned}
 k_{\text{eseal}} &= 7 \text{ BTU/hr ft R} && (\text{Incone1}) \\
 A_{\text{eseal}} &= 2.25'' (0.008'') \pi \\
 L_{\text{eseal}} &= (0.156'' \text{ in/e-seal}) (39 \text{ e-seal})
 \end{aligned}$$

$$\begin{aligned}
 \frac{k_k A_k}{L_k} &= \frac{(9 \text{ BTU/hr ft R}) (0.015 \text{ in}^2)}{4.2 \text{ in}} \frac{\text{ft}}{12 \text{ in}} \frac{\text{hr}}{60 \text{ min}} \\
 &= 4.464 \times 10^{-5} \text{ BTU/min R}
 \end{aligned}$$

$$\begin{aligned}
 \frac{K_{\text{eseal}} A_{\text{eseal}}}{L_{\text{eseal}}} &= \frac{(7 \text{ BTU/hr ft R}) (2.25 \text{ in}) (0.008'') \pi}{(0.156 \text{ in/e-seal}) (39 \text{ e-seal})} \frac{\text{ft}}{12 \text{ in}} \frac{\text{hr}}{60 \text{ min}} \\
 &= 9.036 \times 10^{-5} \text{ BTU/min R}
 \end{aligned}$$

$$\lambda = \frac{(4.464 + 9.036) \times 10^{-5} \text{ BTU/min R}}{\dot{m} (1 \text{ lbm/min}) (0.24 \text{ BTU/lbm R})}$$

$$\begin{aligned}
 \lambda &= \frac{5.63 \times 10^{-4}}{\dot{m} (1 \text{ lbm/min})} && (\text{For air}) \\
 &= \frac{1.09 \times 10^{-4}}{\dot{m} (1 \text{ lbm/min})} && (\text{For helium})
 \end{aligned}$$

4. COLBURN MODULUS (j-factor)

The definition of the Colburn modulus follows:

$$\begin{aligned}
 j &= N_{ST} N_{Pr}^{2/3} && (\text{A10}) \\
 &= \frac{h}{G c_p} N_{Pr}^{2/3}
 \end{aligned}$$

$$\text{But } N_{tu} = \frac{hA}{\dot{m}c_p}$$

$$h = \frac{N_{tu} \dot{m} c_p}{A}$$

$$j = \frac{N_{tu} \dot{m} c_p}{G c_p A} N_{Pr}^{2/3}$$

$$j = N_{tu} \frac{A_c}{A} N_{Pr}^{2/3} \quad (A11)$$

Where:

N_{tu} = Heat-transfer units.

A_c = Minimum free flow area.

A = Total heat-transfer surface area.

N_{Pr} = Prandtl number.

j = Colburn modulus.

5. FRICTION FACTOR

$$f = \frac{D_h \Delta P g_c}{2 \dot{m}^2 \rho V^2}$$

$$\text{But } \dot{m} = \rho A_c V$$

$$f = \frac{D_h \Delta P \rho A_c^2 g_c}{2 \dot{m}^2} \quad (A12)$$

Where:

- f = Friction factor.
- ΔP = Pressure change across the test section.
- n = Number of plates.
- t = Plate thickness.
- g_c = Proportionality factor in Newton's second law.

Tables A1-A5 present the reduced data. Tables A1 and A2 present the friction factor data, Tables A3 and A4 present the heat-transfer data collected using the modified apparatus, and Table A5 presents the heat-transfer data collected using the unmodified apparatus. The EBD and punched core tests were run with different plate orientations. The core descriptions in Tables A1-A5 refer to the following plate orientations:

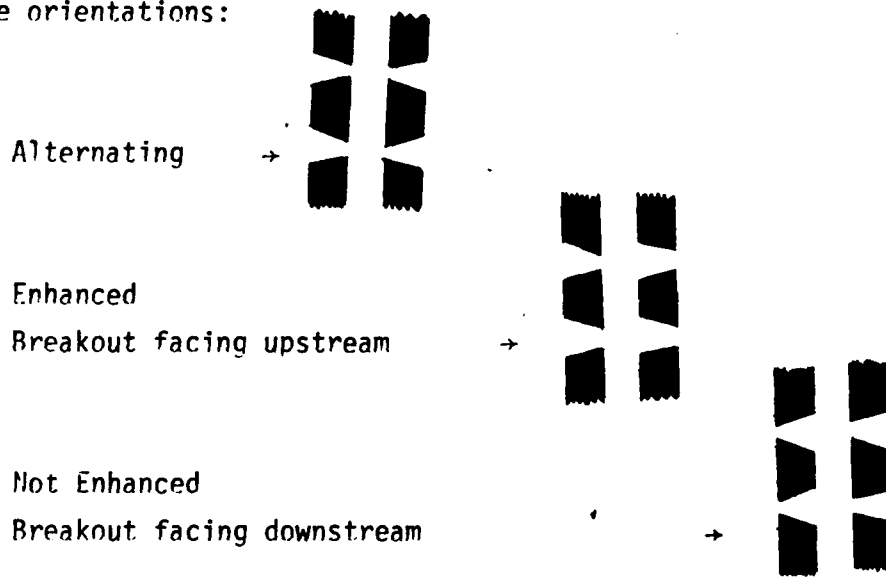


Figure A1 is a sample time/temperature plot for one run.

Run	\dot{m} ($\frac{\text{lbm}}{\text{min}}$)	ΔP ("H ₂ O)	t_{fluid} (°F)	N_{Re}	f	GAS	Core Description
1	0.025	0.09	76.0	4.29	9.52	Air	Punched Plate
2	0.049	0.13	76.0	8.57	3.44		
3	0.099	0.19	76.0	17.15	1.26		
4	0.173	0.38	76.0	29.99	0.82		
5	0.247	0.59	76.0	42.85	0.63		
6	0.119	0.24	76.0	20.57	1.10		
7	0.237	0.57	76.0	41.13	0.66		
8	0.356	1.03	76.0	61.70	0.53		
9	0.474	1.70	76.0	82.25	0.49		
10	0.911	4.65	76.0	158.11	0.36		
11	0.075	0.12	75.0	13.0	1.39		Breakout facing downstream
12	0.100	0.16	75.0	17.34	1.04		
13	0.120	0.23	75.0	20.80	1.04		
14	0.239	0.55	75.0	41.61	0.62		
15	0.335	0.91	75.0	58.24	0.52		
16	0.479	1.65	75.0	83.20	0.47		
19	0.018	0.77	70.0	25.60	1.43	Helium	Etched Plate $d=0.0285"$ $t=0.0185"$ $\sigma=0.09$
20	0.072	1.75	70.0	51.21	0.81		
21	0.108	3.20	70.0	76.80	0.66		
22	0.126	4.30	70.0	89.60	0.65		
23	0.162	6.50	70.0	115.21	0.60		
24	0.025	0.10	75.0	18.04	1.81	Air	
25	0.050	0.16	75.0	36.06	1.08		
26	0.075	0.25	75.0	54.12	0.77		
27	0.100	0.39	75.0	72.16	0.68		
28	0.125	0.55	75.0	90.27	0.61		
29	0.150	0.73	75.0	108.31	0.56		
30	0.175	0.93	75.0	126.35	0.52		
31	0.183	0.99	75.0	131.76	0.51		
32	0.192	1.16	75.0	138.62	0.55		
33	0.240	1.70	75.0	173.25	0.51		
34	0.360	3.57	75.0	259.92	0.48		
35	0.432	5.08	75.0	311.87	0.47		
36	0.480	6.31	75.0	346.51	0.48		
37	0.923	18.20	75.0	666.1	0.37		

Table A1. Friction factor data - punched and etched plates (40 plates/core)

Run	\dot{m} ($\frac{\text{lbm}}{\text{min}}$)	ΔP ("H ₂ O)	t_{fluid} (°F)	N_{Re}	f	GAS	Core Description
1	0.0508	0.07	69.0	16.1	2.727	Air	Etched Plate d=0.0295" t=0.0185" σ=0.245
2	0.1016	0.14	69.0	32.21	1.364		
3	0.1523	0.24	69.0	48.31	1.039		
4	0.2031	0.34	69.0	64.41	0.828		
5	0.2539	0.45	69.0	80.52	0.701		
6	0.0487	0.07	69.0	15.46	2.961		
7	0.0975	0.14	69.0	30.91	1.480		
8	0.1949	0.33	69.0	61.82	0.872		
9	0.2924	0.56	69.0	92.73	0.658		
10	0.3898	0.85	69.0	123.60	0.562		
11	0.4873	1.21	69.0	154.60	0.512		

Table A1. Concluded

Run	\dot{m} ($\frac{\text{lbm}}{\text{min}}$)	ΔP ("H ₂ O)	t_{fluid} (°F)	N_{Re}	f	GAS	Core Description
1	0.929	6.14	70.0	117.3	0.081	Air	24 Plates d=0.010" t=0.065" $\sigma=0.20$ Alternating Pattern
2	0.742	4.12	70.0	93.6	0.085		
3	0.481	2.67	70.0	60.7	0.131		
4	0.433	2.3	70.0	54.6	0.140		
5	0.385	1.94	70.0	48.5	0.149		
6	0.336	1.63	70.0	42.5	0.164		
7	0.288	1.34	70.0	36.4	0.183		
8	0.240	1.07	70.0	30.3	0.211		
9	0.192	0.82	70.0	24.2	0.252		
10	0.144	0.60	70.0	18.2	0.328		
11	0.096	0.39	70.0	12.1	0.480		
12	0.048	0.21	70.0	6.1	1.03		
13	0.125	0.50	70.0	15.8	0.363		
14	0.100	0.04	70.0	12.6	0.442		
15	0.075	0.30	70.0	9.5	0.605		
16	0.050	0.20	70.0	6.3	0.908		
17	0.025	0.12	70.0	3.2	2.2		
69	0.940	8.42	73.0	118.1	0.121		32 Plates d=0.010" t=0.045" $\sigma=0.20$ Not Enhanced
70	0.749	5.60	73.0	94.2	0.126		
71	0.486	3.73	73.0	61.1	0.199		
72	0.437	3.22	73.0	55.0	0.213		
73	0.389	2.74	73.0	48.8	0.229		
74	0.340	2.30	73.0	42.7	0.251		
75	0.291	1.88	73.0	36.6	0.280		
76	0.242	1.50	73.0	30.5	0.322		
77	0.194	1.16	73.0	24.4	0.389		
78	0.145	0.83	73.0	18.3	0.495		
79	0.097	0.55	73.0	12.2	0.738		
80	0.048	0.29	73.0	6.1	1.557		
81	0.126	0.70	73.0	15.9	0.554		
82	0.101	0.55	73.0	12.7	0.680		
83	0.076	0.40	73.0	9.5	0.879		
84	0.050	0.28	73.0	6.3	1.384		
85	0.025	0.14	73.0	3.2	2.770		

Table A2. Friction factor data - ERD plates

Run	\dot{m} ($\frac{\text{lbm}}{\text{min}}$)	ΔP ("H ₂ O)	t_{fluid} (°F)	N_{Re}	f	GAS	Core Description
52	0.837	8.02	75.0	157.3	0.176	Air	27 Plates d=0.015" t=0.065" σ=0.20 Not Enhanced
53	0.742	5.89	75.0	139.4	0.164		
54	0.481	3.68	75.0	90.4	0.243		
55	0.433	3.14	75.0	81.3	0.256		
56	0.384	2.62	75.0	72.3	0.271		
57	0.336	2.16	75.0	63.2	0.292		
58	0.288	1.76	75.0	54.1	0.324		
59	0.240	1.39	75.0	45.1	0.368		
60	0.192	1.06	75.0	36.1	0.439		
61	0.144	0.75	75.0	27.0	0.533		
62	0.096	0.47	75.0	18.0	0.779		
63	0.048	0.24	75.0	9.0	1.592		
64	0.125	0.61	75.0	23.5	0.596		
65	0.100	0.47	75.0	18.8	0.718		
66	0.075	0.34	75.0	14.1	0.923		
67	0.050	0.25	75.0	9.4	1.527		
68	0.025	0.12	75.0	4.7	2.933		
18	0.923	8.58	75.0	231.3	0.203		27 Plates d=0.020" t=0.065" σ=0.20 Enhanced
19	0.735	5.48	75.0	184.3	0.204		
20	0.477	3.52	75.0	119.6	0.310		
21	0.429	2.98	75.0	107.5	0.324		
22	0.381	2.46	75.0	95.5	0.339		
23	0.333	2.0	75.0	83.5	0.360		
24	0.286	1.6	75.0	71.6	0.392		
25	0.238	1.24	75.0	59.6	0.438		
26	0.190	0.92	75.0	47.7	0.508		
27	0.143	0.65	75.0	35.7	0.639		
28	0.095	0.41	75.0	23.8	0.907		
29	0.048	0.20	75.0	11.9	1.77		
30	0.124	0.52	75.0	31.0	0.678		
31	0.100	0.40	75.0	24.8	0.815		
32	0.074	0.30	75.0	18.6	1.086		
33	0.050	0.20	75.0	12.4	1.630		
34	0.025	0.10	75.0	6.20	3.260		

Table A2. Continued

Run	\dot{m} ($\frac{\text{lbm}}{\text{min}}$)	ΔP ("H ₂ O)	t_{fluid} (°F)	N_{Re}	f	GAS	Core Description
35	0.922	8.28	75.0	231.2	0.196	Air	27 Plates d=0.020" t=0.065" $\sigma=0.20$ Not Enhanced
36	0.735	5.26	75.0	184.3	0.196		
37	0.477	3.17	75.0	119.5	0.279		
38	0.429	2.66	75.0	107.5	0.290		
39	0.381	2.21	75.0	95.5	0.305		
40	0.333	1.79	75.0	83.5	0.323		
41	0.286	1.44	75.0	71.6	0.353		
42	0.238	1.12	75.0	59.6	0.396		
43	0.190	0.84	75.0	47.7	0.464		
44	0.143	0.59	75.0	35.7	0.580		
45	0.095	0.37	75.0	23.8	0.818		
46	0.048	0.19	75.0	11.9	1.681		
47	0.124	0.48	75.0	31.0	0.626		
48	0.099	0.38	75.0	24.8	0.774		
49	0.074	0.28	75.0	18.6	1.014		
50	0.50	0.19	75.0	12.4	1.548		
51	0.245	0.10	75.0	6.2	3.260		
86	0.930	6.32	77.0	174.3	0.138	32 Plates d=0.015" t=0.045" $\sigma=0.20$ Alternating Patterns	
87	0.742	4.14	77.0	139.1	0.141		
88	0.482	2.61	77.0	90.3	0.211		
89	0.433	2.20	77.0	81.2	0.220		
90	0.385	1.85	77.0	72.2	0.234		
91	0.337	1.53	77.0	63.1	0.253		
92	0.288	1.23	77.0	54.1	0.277		
93	0.240	0.97	77.0	45.1	0.315		
94	0.192	0.73	77.0	36.0	0.370		
95	0.144	0.54	77.0	27.0	0.487		
96	0.096	0.34	77.0	18.0	0.690		
97	0.048	0.18	77.0	9.0	1.461		
98	0.125	0.42	77.0	23.5	0.502		
99	0.100	0.34	77.0	18.8	0.635		
100	0.075	0.25	77.0	14.1	0.831		
101	0.050	0.18	77.0	9.4	1.346		
102	0.025	0.10	77.0	4.7	2.991		

Table A2. Continued

Run	$\eta \left(\frac{\text{lbm}}{\text{min}} \right)$	$\Delta P (\text{"H}_2\text{O})$	$t_{\text{fluid}} (\text{°F})$	N_{Re}	f	GAS	Core Description	
103	0.926	5.99	77.0	231.5	0.174	Air	32 Plates d=0.020" t=0.045" $\sigma=0.20$ Alternating Patterns	
104	0.739	3.95	77.0	184.7	0.180			
105	0.480	2.38	77.0	119.9	0.256			
106	0.432	1.99	77.0	107.9	0.265			
107	0.383	1.64	77.0	95.8	0.277			
108	0.335	1.33	77.0	83.8	0.293			
109	0.287	1.05	77.0	71.8	0.315			
110	0.239	0.81	77.0	59.8	0.350			
111	0.191	0.60	77.0	47.9	0.406			
112	0.144	0.41	77.0	35.9	0.493			
113	0.096	0.26	77.0	23.9	0.704			
114	0.048	0.13	77.0	12.0	1.407			
115	0.125	0.34	77.0	31.2	0.542			
116	0.100	0.26	77.0	24.9	0.648			
117	0.075	0.19	77.0	18.7	0.842			
118	0.050	0.13	77.0	12.5	1.296			
119	0.025	0.07	77.0	6.2	2.792			
120	0.941	6.71	68.0	119.1	0.223			31 Plates d=0.010" t=0.020" $\sigma=0.20$ Alternating Patterns
121	0.751	5.19	68.0	95.1	0.269			
122	0.487	2.97	68.0	61.7	0.366			
123	0.438	2.54	68.0	55.5	0.386			
124	0.389	2.12	68.0	49.3	0.408			
125	0.341	1.68	68.0	43.1	0.423			
126	0.292	1.44	68.0	36.9	0.493			
127	0.243	1.15	68.0	30.8	0.563			
128	0.194	0.88	68.0	24.6	0.679			
129	0.146	0.63	68.0	18.4	0.864			
130	0.097	0.42	68.0	12.3	1.296			
131	0.049	0.21	68.0	6.1	2.594			
132	0.253	1.18	68.0	32.1	0.536			
133	0.288	1.0	68.0	28.8	0.578			
134	0.203	0.9	68.0	25.6	0.639			
135	0.177	0.78	68.0	22.4	0.724			
136	0.152	0.64	68.0	19.2	0.808			
137	0.126	0.53	68.0	16.0	0.964			
138	0.101	0.40	68.0	12.8	1.137			
139	0.076	0.31	68.0	9.6	1.567			
140	0.051	0.21	68.0	6.4	2.389			
141	0.025	0.11	68.0	3.2	5.006			

Table A2. Continued

Run	\dot{m} ($\frac{\text{lbm}}{\text{min}}$)	ΔP ("H ₂ O)	t_{fluid} (°F)	N_{Re}	f	GAS	Core Description
142	0.933	6.63	70.0	176.6	0.354	Air	29 Plates
143	0.744	3.97	70.0	140.8	0.332		
144	0.483	2.38	70.0	91.4	0.472		$d=0.015"$
145	0.434	1.99	70.0	82.2	0.487		$t=0.020"$
146	0.386	1.64	70.0	73.1	0.509		$\sigma=0.20$
147	0.338	1.32	70.0	63.9	0.535		
148	0.289	1.05	70.0	54.8	0.579		Alternating
149	0.241	0.82	70.0	45.6	0.652		Patterns
150	0.193	0.61	70.0	36.5	0.758		
151	0.145	0.42	70.0	27.4	0.928		
152	0.096	0.27	70.0	18.2	1.342		
153	0.048	0.14	70.0	9.1	2.783		
154	0.251	0.85	70.0	47.5	0.622		
155	0.226	0.74	70.0	42.8	0.669		
156	0.201	0.62	70.0	38.0	0.709		
157	0.176	0.52	70.0	33.3	0.777		
158	0.151	0.43	70.0	28.5	0.875		
159	0.125	0.34	70.0	23.8	0.996		
160	0.100	0.26	70.0	19.0	1.190		
161	0.075	0.19	70.0	14.2	1.546		
162	0.050	0.13	70.0	9.5	2.381		
163	0.025	0.07	70.0	4.7	5.128		

Table A2. Concluded

Run	\dot{m} lbm/min	t_i (°F)	t_{f1} (°F)	Max Slope Parameter	N_{RE}	N_{tu} (total)	N_{tu} per plate	Test Gas	Core Description
21	0.322	81.65	100.8	1.218	55.74	18.170	0.454	Air	Punched Plate breakout upstream d=0.018" t=0.021" $\sigma=0.236$ $N_{tu}=3.60 N_{RE}$
23	0.119	77.96	104.1	1.533	19.91	31.99	0.800		
24	0.476	77.27	92.78	1.160	80.76	16.29	0.407		
25	0.915	78.22	96.0	1.005	154.55	11.88	0.298		
26	0.976	75.96	90.52	1.716	12.88	39.98	1.151		
27	0.100	76.96	97.48	1.492	16.82	30.63	0.766		
28	0.100	77.91	99.91	1.447	16.76	28.47	0.712		
29	0.075	78.09	92.87	1.651	12.67	41.60	1.040		
30	0.119	78.61	105.52	1.453	19.89	28.23	0.706		
32	0.226	76.26	95.52	1.197	56.70	17.65	0.441		
33	0.479	77.55	96.55	1.108	80.89	14.77	0.369		
34	0.922	77.05	93.83	0.939	156.07	10.27	0.257		
36	0.234	76.17	100.25	1.242	39.20	19.12	0.478		
37	0.232	78.26	100.44	1.343	38.94	22.67	0.567		
40	0.2390	79.48	102.65	0.965	166.1	11.00	0.275	Etched plate d=0.0285" t=0.0185" $\sigma=0.09$ $N_{tu}=2.10 N_{RE}$	
41	0.120	79.26	103.61	1.218	82.95	18.82	0.471		
42	0.334	79.65	104.13	0.938	231.5	10.28	0.257		
43	0.476	76.48	98.26	0.933	332.8	10.16	0.254		
46	0.074	78.65	98.35	1.226	51.82	19.77	0.494		
49	0.100	70.16	95.39	1.212	70.16	18.80	0.470		
52	0.924	74.35	92.39	0.837	650.83	7.98	0.198		
53	0.919	75.27	93.04	0.839	646.8	7.98	0.199		
54	0.125	77.27	100.25	1.183	85.58	16.94	0.423		
55	0.048	76.26	99.74	1.414	32.69	25.31	0.633		
56	0.018	76.13	90.13	1.475	12.28	30.10	0.753		
57	0.238	75.64	100.38	0.936	165.79	10.26	0.256		

Table A3. Heat-transfer data - punched and etched plates (40 plates/core)

Run	\dot{m} $\frac{\text{lbm}}{\text{min}}$	t_i ($^{\circ}\text{F}$)	f_1 ($^{\circ}\text{F}$)	Max Slope Parameter	N_{RE}	N_{tu} (total)	N_{tu} per plate	Test Gas	Core Description
1	0.101	73.0	93.7	1.279	30.99	21.13	0.508	Air	Etched plate d=0.0295" t=0.0185" $\sigma=0.245$ $N_{tu}=4.13 N_{RE}^{-0.594}$
2	0.121	72.7	96.7	1.263	37.04	20.53	0.494		
3	0.360	72.3	94.1	0.976	110.3	11.15	0.279		
4	0.482	72.5	92.4	0.848	148.0	8.18	0.205		
5	0.240	72.3	97.1	0.962	73.16	11.08	0.271		
6	0.169	75.4	99.1	1.224	51.44	19.12	0.456		

Table A3. Concluded

Run	\dot{m} $\frac{\text{lbm}}{\text{min}}$	t_i ($^{\circ}\text{F}$)	T_f ($^{\circ}\text{F}$)	Max Slope Parameter	N_{RE}	N_{tu} (total)	N_{tu} per plate	Test Gas	Core Description
1	0.097	70.6	97.9	1.193	11.8	17.52	0.730	Air	24 plates $t=0.065"$ $d=0.010"$ $\sigma=0.20$ Alternating pattern $N_{tu}=0.993 N_{RE}$ -0.093
2	0.752	71.9	94.3	1.088	91.8	14.0	0.582		
3	0.390	74.5	94.5	1.245	47.6	18.83	0.785		
4	0.390	73.1	99.5	1.240	29.7	18.73	0.780		
5	0.498	71.8	87.7	1.297	61.3	20.49	0.854		
6	0.296	72.0	95.7	1.231	36.0	18.40	0.767		
7	0.169	72.0	100.6	1.190	20.5	17.24	0.718		
28	0.484	79.5	95.1	1.213	59.0	17.80	0.556	Air	32 plates $t=0.045"$ $d=0.010"$ $\sigma=0.20$ Not enhanced $N_{tu}=0.989 N_{RE}$ -0.168
29	0.389	78.0	97.9	1.332	49.3	21.7	0.678		
30	0.094	78.3	106.3	1.222	11.3	18.45	0.577		
31	0.290	78.7	104.9	1.280	34.9	20.01	0.625		
32	0.244	79.9	109.0	1.167	29.3	16.47	0.515		
33	0.166	78.6	110.3	1.247	19.8	19.06	0.596		
34	0.934	82.1	94.4	1.011	114.0	12.05	0.377		
35	0.746	82.9	99.4	1.055	90.4	13.15	0.411		
8	0.169	77.3	114.7	1.107	30.2	14.75	0.546	Air	27 plates $t=0.065"$ $d=0.015"$ $\sigma=0.20$ Not enhanced $N_{tu}=1.66 N_{RE}$ -0.291
9	0.242	77.6	106.2	1.101	43.5	14.54	0.539		
10	0.286	76.5	100.6	1.031	51.9	12.6	0.467		
11	0.381	76.9	95.8	1.153	69.5	16.0	0.593		
12	0.488	78.5	93.0	1.069	89.5	13.60	0.504		
13	0.096	77.6	103.9	1.281	17.4	20.48	0.759		
14	0.738	81.2	98.9	0.963	134.3	10.84	0.401		
15	0.829	81.3	97.3	0.887	151.0	9.05	0.335		

Table A4. Heat-transfer data - EBN plates

Run	\dot{m} $\frac{\text{lbm}}{\text{min}}$	t_i ($^{\circ}\text{F}$)	t_{f1} ($^{\circ}\text{F}$)	Max Slope Parameter	N_{RE}	N_{tu} (total)	N_{tu} per plate	Test Gas	Core Description
16	0.167	81.6	113.6	1.204	39.7	17.67	0.654	Air	27 plates Enhanced $t=0.065''$ $d=0.020''$ $\sigma=0.20$ $N_{tu}=1.60 N_{RE}$ -0.237
17	0.283	80.2	107.5	1.152	67.9	15.99	0.592		
18	0.478	78.9	95.0	1.101	116.6	14.50	0.537		
19	0.914	83.2	91.3	0.995	223.9	11.64	0.431		
20	0.096	76.1	104.0	1.255	23.2	19.58	0.725		
21	0.168	78.5	109.6	1.236	40.1	18.72	0.693		
22	0.241	78.3	107.0	1.075	57.8	13.80	0.511		
23	0.289	78.5	104.7	1.081	69.7	13.96	0.517		
24	0.382	79.0	99.5	1.050	92.7	13.07	0.484		
25	0.488	78.8	93.8	0.996	119.3	11.68	0.432		Not enhanced $N_{tu}=1.98 N_{RE}$ -0.313
26	0.736	80.6	94.0	0.931	179.7	10.06	0.373		
27	0.916	81.2	90.6	0.946	224.7	10.41	0.386		
36	0.925	79.8	94.8	1.033	169.3	12.60	0.394		32 plates $t=0.045''$ $d=0.015''$ $\sigma=0.20$ Alternating pattern $N_{tu}=2.03 N_{RE}$ -0.313
37	0.738	81.6	101.1	1.010	133.9	12.02	0.375		
38	0.097	81.8	119.6	1.392	17.1	24.55	0.767		
39	0.482	81.5	98.4	1.259	87.8	19.25	0.602		
40	0.382	82.1	103.3	1.264	69.1	19.44	0.607		
41	0.167	79.0	112.3	1.404	30.0	24.59	0.768		
42	0.229	79.2	110.5	1.254	41.2	19.23	0.601		
43	0.293	79.7	107.7	1.197	52.7	17.35	0.542		
44	0.919	80.6	94.2	0.908	224.2	9.53	0.298		32 plates $t=0.045''$ $d=0.020''$ $\sigma=0.20$ Alternating patterns $N_{tu}=3.23 N_{RE}$ -0.435
45	0.739	97.8	97.8	0.934	179.6	10.14	0.317		
46	0.100	79.0	108.8	1.338	23.9	22.46	0.702		
47	0.482	78.5	95.8	1.056	117.3	13.24	0.414		
48	0.382	79.6	101.3	1.087	92.4	14.12	0.441		
49	0.167	80.0	111.4	1.368	39.9	23.25	0.727		
50	0.285	79.5	105.3	1.224	68.5	18.21	0.569		
51	0.230	78.7	104.2	1.220	57.5	18.10	0.566		

Table A4. Continued

Run	\dot{m} $\frac{\text{lbm}}{\text{min}}$	t_j ($^{\circ}\text{F}$)	T_1 ($^{\circ}\text{F}$)	Max Slope Parameter	N_{RE}	N_{tu} (total)	N_{tu} per plate	Test Gas	Core Description
52	0.939	78.6	97.6	0.930	114.1	10.04	0.324	Air	31 plates $t=0.020"$ $d=0.010"$ $\sigma=0.20$ Alternating patterns $N_{tu}=2.52 N_{RE}$ -0.428
53	0.750	75.8	93.0	0.975	91.7	11.13	0.359		
54	0.101	73.1	99.7	0.406	12.2	25.04	0.808		
55	0.486	72.5	88.5	1.095	59.8	14.33	0.462		
56	0.288	73.2	98.4	1.163	35.0	16.35	0.527		
57	0.166	72.5	100.6	1.387	20.0	23.93	0.772		
58	0.241	72.3	100.1	1.231	29.2	18.47	0.596		
59	0.095	72.4	98.7	1.377	17.3	23.99	0.827		
60	0.477	74.9	91.6	1.076	87.7	13.79	0.475		
61	0.169	72.5	102.1	1.350	30.7	22.6	0.779		
62	0.933	73.1	89.8	0.859	11.8	8.43	0.291		
63	0.242	72.0	102.2	1.117	43.9	15.00	0.517		
64	0.743	74.2	94.2	0.873	136.1	8.73	0.301		
65	0.291	74.3	98.5	1.019	52.9	12.29	0.424		
									29 plates $t=0.020"$ $d=0.015"$ $\sigma=0.20$ Alternating patterns $N_{tu}=3.36 N_{RE}$ -0.477

Table A4. Concluded

Run	\dot{m} lbm/min	t_i (°F)	t_{f1} (°F)	Max Slope Parameter	N_{RE}	N_{tu} (total)	N_{tu} per plate	Core Description
1	0.3327	76.043	133.917	1.2165	53.68	17.806	0.445	$N_{tu}=2.02 N_{RE}^{-0.403}$ $d=0.018"$ $t=0.021"$ $\sigma=0.236$
2	0.320	75.454	132.917	1.087	51.69	14.041	0.351	
3	0.2366	83.435	107.667	1.126	39.37	15.143	0.379	
4	0.1201	75.409	99.783	1.224	10.18	18.462	0.462	
5	0.4805	80.955	129.958	1.173	77.88	16.507	0.413	
6	0.0999	80.545	107.208	1.504	16.63	28.892	0.722	
7	0.4774	77.909	130.083	1.163	77.37	16.209	0.405	
8	0.333	78.348	123.667	1.359	54.42	22.421	0.561	
9	0.1192	75.545	101.609	1.436	19.98	26.144	0.654	
10	0.2378	77.455	108.435	1.241	39.53	18.800	0.470	
11	0.0991	78.957	109.5	1.389	16.454	24.314	0.608	
12	0.051	75.864	93.652	1.443	8.64	27.443	0.686	
13	0.0247	79.043	87.348	1.838	4.223	61.051	1.526	
14	0.9190	77.455	112.435	0.9793	152.05	11.241	0.281	
15	0.2390	78.478	112.739	1.202	39.53	17.360	0.434	
16	0.3368	76.870	118.583	0.966	55.32	10.902	0.273	
17	0.3368	77.5	117.565	1.102	55.388	14.486	0.362	
18	0.3368	78.0	118.563	1.154	55.32	15.943	0.399	
19	0.3334	81.783	122.75	1.219	54.50	17.881	0.447	
20	0.3327	81.478	110.435	1.1817	55.178	16.767	0.419	

Table A5. Heat-transfer data - punched plate tested with air; original apparatus

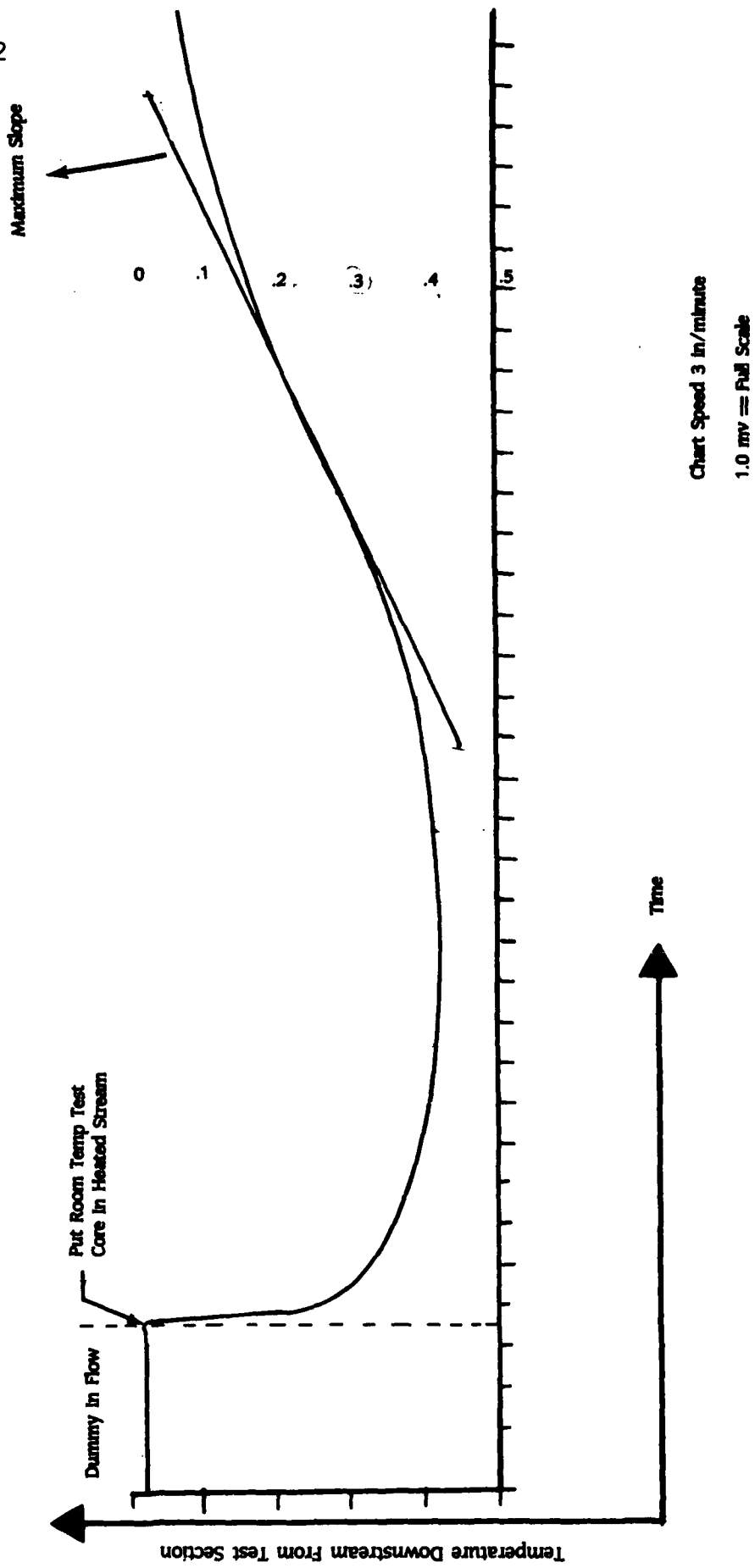


Figure A2. Temperature of air downstream from test section as a function of time (run #21)

APPENDIX B - ACCURACY

Both the experimental errors inherent to the single blow transient test method and the inaccuracies particular to the experimental set up have been considered [1] to estimate the following uncertainties:

Quantity		Maximum Uncertainty (percent)
N_{Pr}	Prandtl Number	± 5.0
$c_{p \text{ air}}$	Specific heat	± 0.5
μ_{air}	Dynamic viscosity	± 1.0
C_{air}	Specific heat	± 4.0
D_h^{copper}	Hydraulic diameter	± 2.0
N_h	Hole Reynolds number	± 9.0
f_{Re}	friction factor	± 10.0
N_{tu}	Number of heat-transfer units	± 20.0

Table B1. Maximum uncertainty of physical constants and measurements

With regard to equipment inaccuracies, some verification of actual performance was made where possible. Thermocouples were checked and found to give accuracies of ± 0.1 °F. Three Fisher-Porter rotometers were used to determine mass flows. The smallest meter was checked with a wet-test meter and found to be accurate to within 5 percent. The estimation of maximum slope itself has an error which varies according to the range of Reynolds number under consideration. At low Reynolds numbers ($N_{Re} \sim 20$) the possible error in reading maximum slope means a ± 6 percent variation in N_{tu} per plate. At higher Reynolds numbers this reduces to ± 3 percent. By digitizing the time-temperature profile through the use of a minicomputer this error could be reduced to less than ± 1 percent. This was done for the eight electron beam drilled plates.

APPENDIX C - MODELING THE PLATE

An analytical model of the plate was developed to evaluate the experimental data. The fin effectiveness for a circular fin, the effective thermal conductivity, the friction factor vs hole Reynolds number, and the number of heat-transfer units per plate vs hole Reynolds number were determined analytically.

At first the plate was modeled as a "matrix," similar to a porous media, but the correlation parameters generated didn't describe the system correctly. Finally, the plate was modeled using the staggered (hexagonal) hole pattern shown in Figure C1. This model adequately describes the heat exchanger's behavior.

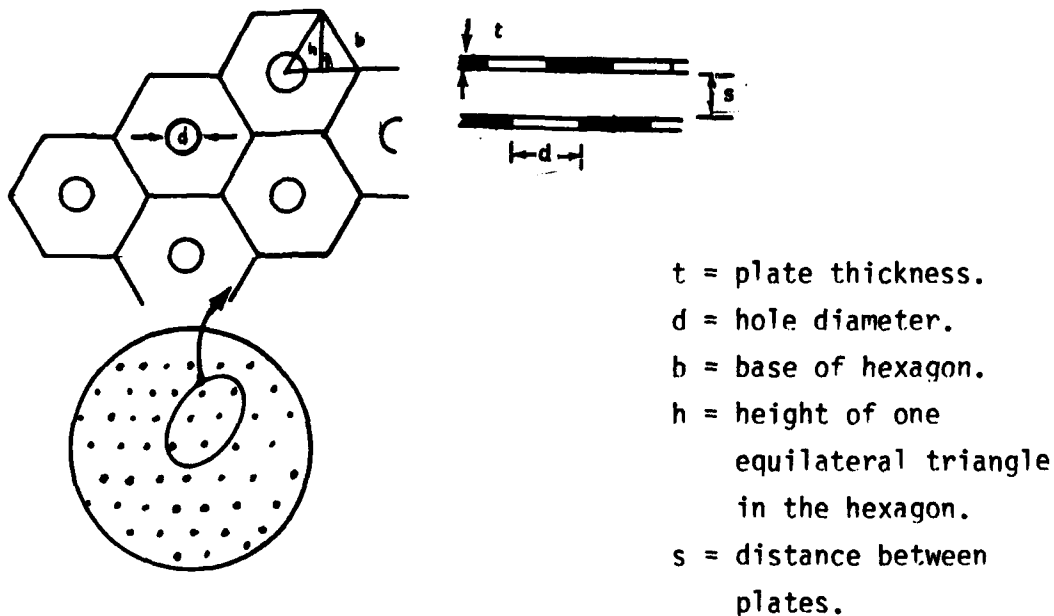


Figure C1. Model of staggered hole pattern

1. DETERMINE FIN EFFECTIVENESS FOR A CIRCULAR FIN

The single-blow transient-test method generates the N_{tu} for a plate with 100% fin effectiveness (η_f) because each plate is at a constant temperature at any given time during the test. The fin effectiveness must be considered to determine the actual N_{tu}/plate when designing heat exchangers.

$$\frac{1}{N_{tu_{eff}}} = \frac{1}{N_{tu_{LP}} \eta_{f_{LP}}} + \frac{1}{N_{tu_{HP}} \eta_{f_{HP}}} \quad (C1)$$

The two pass counterflow heat exchanger (see Figure 2 and C2) will be designed with a high pressure central core and a low pressure stream in the annular section surrounding the center.

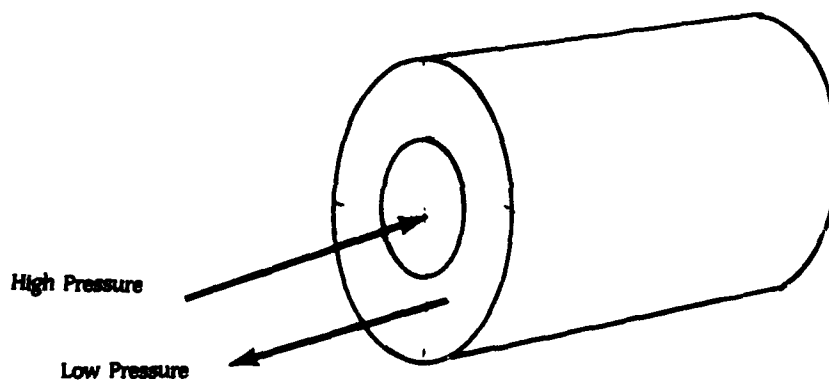


Figure C2. Two pass heat exchanger

Kays and London [3] have evaluated and presented the fin effectiveness for annular flow in Figure 2-11. The fin effectiveness is also needed for the circular center section (high-pressure stream in RCUBE application). The analysis follows.

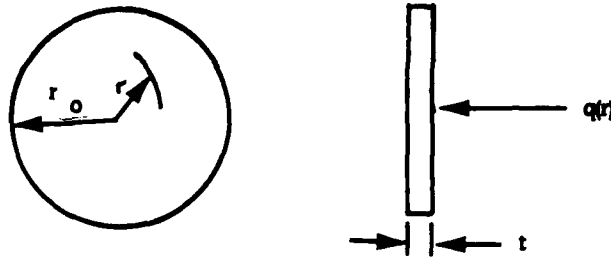


Figure C3. Model of circular fin (high-pressure flow path)

Start with the differential equation describing temperature profile of the fin shown in Figure C3.

$$\frac{d^2T}{dr^2} + \frac{1}{r} \frac{dT}{dr} + \frac{1}{kt} [q(r)] = 0 \quad (C2)$$

where

- T = Temperature at radial location r.
- k = Coefficient of thermal conductivity.
- h = Convective heat transfer coefficient.
- q(r) = Absorbed heat flux.
- = $h[T_g - T]$.
- T_g = Temperature of the gas.

Let

$$T = T_g + \theta \quad \text{and transform eq (C2) to}$$

$$\frac{d^2\theta}{dr^2} + \frac{1}{r} \frac{d\theta}{dr} + \frac{h\theta}{kt} = 0 \quad (C3)$$

To solve the differential equation, the boundary conditions must be determined. Figure C4 shows the temperature profiles for both $T_g < T$ and $T > T_g$.

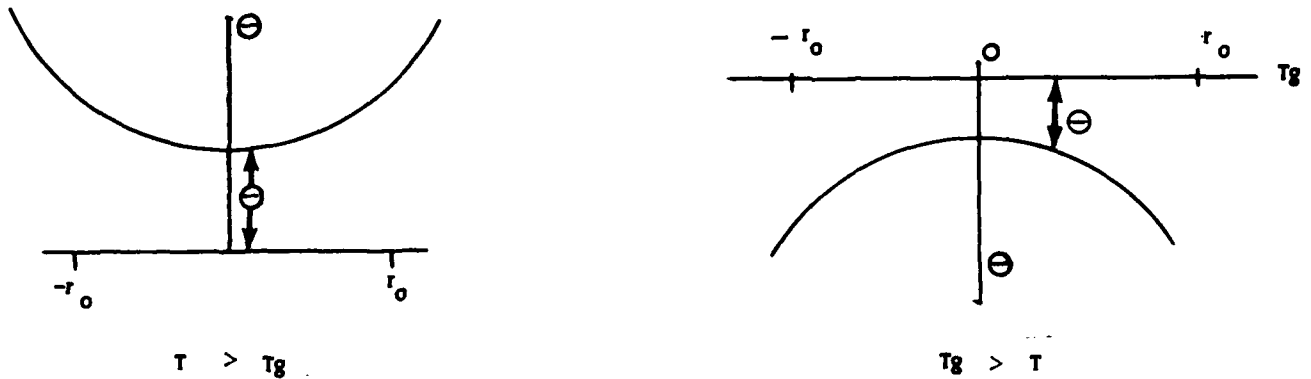


Figure C4. Fin temperature properties

From Figure C4, the following boundary conditions can be seen.

At $r = 0$

$$\frac{d\theta}{dr} = 0; \theta \text{ is finite}$$

At $r = r_0$

First, find $\left. \frac{d\theta}{dr} \right|_{r_0}$

$$q_{r_0} = -k(2\pi)r_0 t \left. \frac{dT}{dr} \right|_{r_0}$$

$$= -k(2\pi r_0 t) \left. \frac{d\theta}{dr} \right|_{r_0} \tag{C4}$$

But, the following relation for q_{r0} is based on the definition of q_{r0} :

$$\begin{aligned}
 q_{r0} &= \int_0^{r_0} h(T_g - T) 2\pi r dr \\
 &= -2\pi h \int_0^{r_0} \theta r dr
 \end{aligned}
 \tag{C5}$$

Substituting equation (C5) into equation (C4):

$$\begin{aligned}
 \frac{d\theta}{dr} \Big|_r &= \frac{2\pi h \int_0^{r_0} \theta r dr}{k(2\pi r_0 t)} \\
 \frac{d\theta}{dr} \Big|_0 &= \frac{h}{kr_0 t} \int_0^{r_0} \theta r dr
 \end{aligned}
 \tag{C6}$$

Since the fin effectiveness is defined as the ratio of the actual heat transferred to the heat that would be transferred if the entire fin was at the base temperature,

$$\eta_f = \frac{\int_0^{r_0} (T - T_g) 2\pi r dr}{\int_0^{r_0} (T_0 - T_g) 2\pi r dr}$$

$$= \frac{\int_0^{r_0} 2\pi r \theta dr}{\pi r_0^2 (T_0 - T_g)}$$

$$\eta_f = \frac{\int_0^{r_0} 2 r \theta dr}{r_0^2 \theta_0}$$

(C7)

Combine equations (C6) and (C7):

$$\eta_f = \frac{2 \frac{d\theta}{dr} \Big|_{r_0} \frac{kr_0 t}{h}}{r_0^2 \theta_0}$$

$$\eta_f = \frac{2k t}{hr_0 \theta_0} \frac{d\theta}{dr} \Big|_{r_0}$$

(C8)

Define u^2 as follows:

$$u^2 = \frac{hr^2}{kt}$$

$$u_0^2 = \frac{hr_0^2}{kt}$$

(C9)

$$\eta_f = \frac{2r_o}{u_o^2} \frac{d\theta|_{r_o}}{dr} \quad (C10)$$

To find $\frac{d\theta}{du}$, use the chain rule

$$\frac{d\theta}{du} = \frac{d\theta}{dr} \frac{dr}{du}$$

and differentiate equation (C9) to find $\frac{dr}{du}$:

$$2u \frac{du}{dr} = \frac{h}{kt} \frac{2r}{dr}$$

$$\frac{dr}{du} = \frac{u}{r} \frac{kt}{h}$$

$$\frac{d\theta|_u}{du} = \frac{d\theta|_r}{dr} \frac{u}{r} \frac{kt}{h}$$

$$= \left(\frac{d\theta}{dr} \Big|_{r_o} \right) \left(\frac{u_o r_o}{u_o^2} \right)$$

$$\frac{d\theta}{dr} \Big|_{r_o} = \frac{u_o}{r_o} \frac{d\theta}{du} \Big|_{u_o} \quad (C11)$$

Substitute equation (C11) in equation (C10):

$$\ddot{\eta}_f = \frac{2r_0}{u_0^2 \theta_0} \frac{u_0}{r_0} \frac{d\theta}{du} \Big|_{u_0}$$

$$\ddot{\eta}_f = \frac{2}{u_0 \theta_0} \frac{d\theta}{du} \Big|_{u_0} \quad (C12)$$

Now, find equation (C2) in terms of u and θ :

First, multiply through by r^2

$$r^2 \frac{d^2\theta}{dr^2} + \frac{rd\theta}{dr} - r^2 \frac{h}{kt} \theta = 0 \quad (C13)$$

Rearrange and differentiate equation (C9).

$$u = \sqrt{\frac{h}{kt}} r$$

$$\frac{du}{dr} = \sqrt{\frac{h}{kt}}$$

$$\frac{d^2u}{dr^2} = 0$$

Use the chain rule to find $\frac{d\theta}{du}$ and $\frac{d^2\theta}{dr^2}$:

$$\frac{d\theta}{dr} = \frac{d\theta}{du} \frac{du}{dr} = \sqrt{\frac{h'}{kt}} \frac{d\theta}{du}$$

$$\frac{d^2\theta}{dr^2} = \frac{d\theta}{du} \frac{d^2u}{dr^2} + \frac{d^2\theta}{du^2} \left(\frac{du}{dr}\right)^2 = \frac{h}{kt} \frac{d^2\theta}{du^2}$$

Now, equation (C13) can be rewritten:

$$u^2 \frac{d^2\theta}{du^2} + u \frac{d\theta}{du} - u^2\theta = 0 \quad (C14)$$

Equation (C14) is the modified Bessel equation ($n=0$) and the solution follows:

$$\theta = c_1 I_0(u) + c_2 K_0(u)$$

Apply the boundary conditions to find the constants.

At $r = 0$, $u = 0$, $\theta = \text{finite}$

Since $K_0(0) = \infty$, $c_2 = 0$.

$$\theta = c_1 I_0(u) \quad (C15)$$

$$\frac{d\theta}{du} = c_1 \frac{d[I_0(u)]}{du} = c_1 I_1(u) \quad (C16)$$

Substitute equations (C15) and (C16) in equation (C12). Equation (C17) is a relationship for the fin effectiveness as a function of the fin (high-pressure center section) radius, the plate thickness, the heat-transfer coefficient, and the thermal conductivity of the plate.

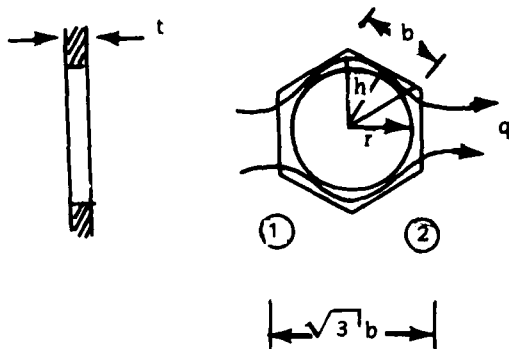
$$\eta_f = \frac{2T_1(u_0)}{u_0 T_0(u_0)}$$

where $u_0 = r_0 \sqrt{\frac{h}{kt}}$

(C17)

2. EVALUATION OF EFFECTIVE VALUES OF THERMAL CONDUCTIVITY

The effective thermal conductivity must be used to calculate fin effectiveness and other heat-transfer characteristics. The holes in the plate cause a lower thermal conductivity than the corresponding material thermal conductivity. The following analysis finds the effective thermal conductivity as a function of percent open area. Consider the flow of a constant amount of heat, q , through the distance $2b$ defined by planes at 1 and 2 (see Figure C2).



t = plate thickness.
 b = one side of hexagon.
 h = height of one equilateral triangle in the hexagon.
 r = radius of hole.
 q = heat flow.

Figure C5. Model of a single hole

The following assumptions were made:

a. There is no heat flow across the boundaries defined by the hexagon (due to symmetry).

b. The heat transfer by solid conduction is isotropic for the integrated effect of the flow area.

The rate of heat conduction for steady one-dimensional conduction follows:

$$q = k A(x) \frac{dT}{dx} \quad (C18)$$

where

q = Rate of heat conduction.

k = Thermal conductivity of the material.

dT/dx = Temperature gradient at the section.

x = Distance along the heat flow lines; defined positive in the direction of the heat flow.

$A(x)$ = Area the heat is flowing through measured perpendicular to the heat flow.

NOTE: The area is a function of x .

Rearrange equation (C18) and integrate:

$$\int_0^{\Delta T} dT = \frac{q}{k} \int_0^{\Delta x} \frac{dx}{A(x)} \quad (C19)$$

$$\Delta T = \frac{q \Delta x}{k} \frac{1}{A(x)|_{av}}$$

where

ΔT = The temperature change across the section from 1 to 2.

Δx = The distance along the heat flow lines from section 1 to 2 (for one cell).

$\frac{1}{A(x)|_{av}}$ = Average value of the reciprocal of the heat flow area.

To determine the effective thermal conductivity,

let $\Delta x = 2b$.

Because the holes are staggered, the area of the two cells must be considered when $\Delta x = 2b$ (see Figure C6).

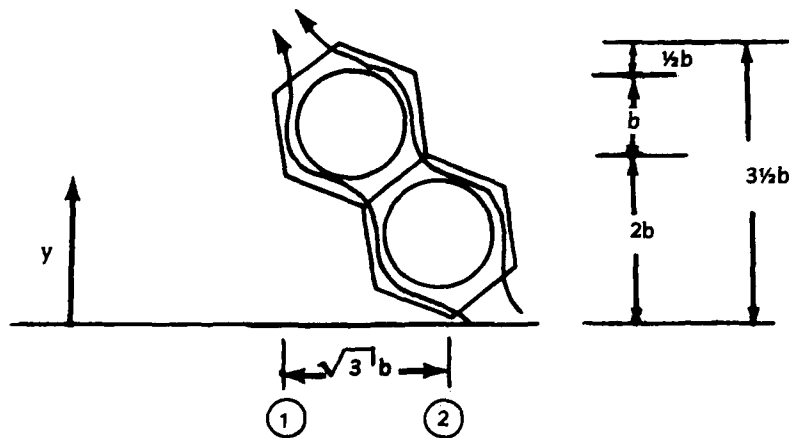


Figure C6. Model of two holes

The average area for the coupled system of holes is twice the area for one hole and the plate thickness is constant; therefore, equation (C19) can be written as follows:

$$\frac{\Delta T}{2b} = \frac{q}{2k} \frac{1}{A(x)|_{av}} = \frac{q}{2kt} \frac{1}{y(x)|_{av}} \quad (C20)$$

where

$y(x)$ = The flow cross section as a function of x
for both parallel flow paths
(see Figures C5 and C7).

Equation (C20) uses the actual area and the actual thermal conductivity. The effective thermal conductivity is defined as the thermal conductivity that would be needed to give the same results as equation (C20) if there were no holes. If the effective thermal conductivity and the area assuming no holes are used in equation (C19), the following equation results:

$$\frac{\Delta T}{2b} = \frac{q}{3.5tbk'} \quad (C21)$$

where

k' = effective thermal conductivity

Next, find the ratio of effective to actual thermal conductivity by combining equations (C17) and (C21).

$$\frac{k'}{k} = \frac{2}{3.5b} \frac{1}{y(x)|_{av}} \quad (C22)$$

Now, if $[y(x)]_{av}$ is redefined to be the cross section for a single parallel flow path instead of both parallel flow paths as shown in Figure C2, equation (C5) will become

$$\frac{k'}{k} = \frac{4}{3.5b \frac{1}{[y(x)]_{av}}} \quad (C23)$$

The relationship of k'/k as needed as a function of a plate's open area ratio (σ). To find k'/k as a function of σ , $\frac{1}{[y(x)]_{av}}$ must be found as a function of σ . First, consider a sixth of a hole and the equilateral triangle associated with it (see Figure C7).

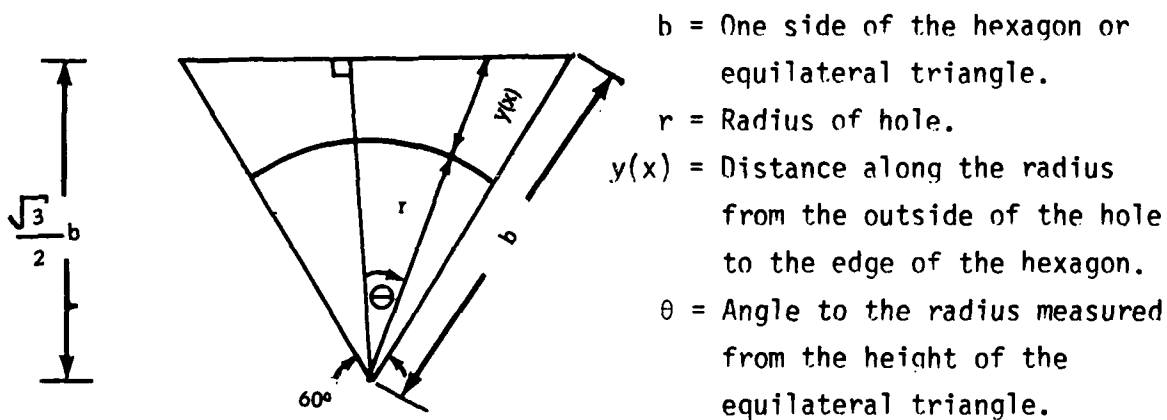


Figure C7. Model of a sixth of a hole

The hole geometry determines $\cos\theta$.

$$\cos\theta = \frac{\frac{\sqrt{3}}{2} b}{r + y(x)} \quad (C24)$$

$$y(x) = \frac{\sqrt{3} / 2 \cdot b}{\cos \theta} - r$$

$$\frac{b}{y(x)} = \frac{1}{\sqrt{3}/2 - r/b} \quad (C25)$$

Now, r/b must be found as a function of σ . σ is the ratio of plate open area to plate frontal area and is also the ratio of the area of one hole to the hexagon surrounding that hole.

$$\sigma = \frac{\pi r^2}{6[(1/2)b][(\sqrt{3}/2)b]} = \frac{2\pi r^2}{3\sqrt{3} b^2}$$

$$r/b = 0.9094 \sigma^{1/2} \quad (C26)$$

Substituting equation (C26) in equation (C25) results in the following relationship:

$$\frac{b}{y(x)} = \left(\frac{\sqrt{3}/2}{\cos \theta} - 0.9094 \sqrt{\sigma} \right)^{-1} \quad (C27)$$

For any given σ , $\frac{b}{y(x)|_{av}}$ can be found by taking the average value for $0 \leq \theta \leq 30$.

$$\frac{b}{y(x)|_{av}} = \frac{6}{\pi} \int_0^{\pi/6} \frac{(\sqrt{3}/2 - 0.9094\sqrt{\sigma^1})^{-1}}{\cos\theta} d\theta \quad (C28)$$

Solving equation (C28) for various values of σ and plugging the result into equation (C22) will generate k'/k (σ). Figure C8 shows k'/k plotted vs σ .

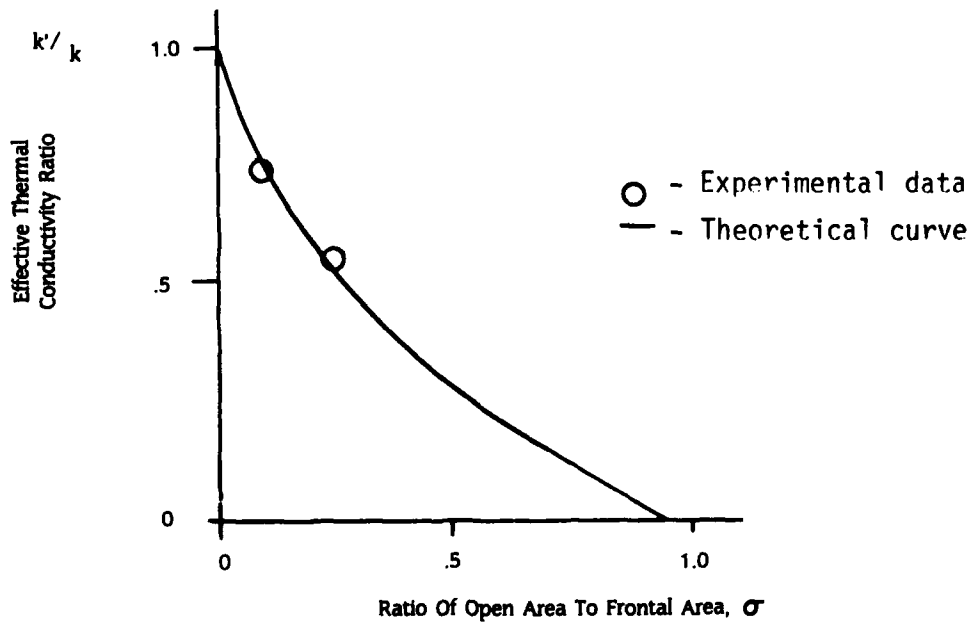


Figure C8. Plot of effective thermal conductivity ratio vs plate open area ratio

As the open area approaches zero, k'/k approaches unity as it should; it doesn't go exactly to one because of the approximations involved in the system analysis.

This analysis was confirmed experimentally by using the following analogue between thermal conductivity and electricity:

$$\frac{k'}{k} = \frac{V_{\text{solid}}}{V} \quad (C29)$$

where:

V_{solid} = Voltage across solid material for a given current.

V = Voltage across perforated material for the same current.

3. DETERMINE FRICTION FACTOR vs HOLE REYNOLDS NUMBER

A single plate will be considered to find the friction factor for the entire core. Figure C9 shows the plate to be considered and the corresponding pressure drops.

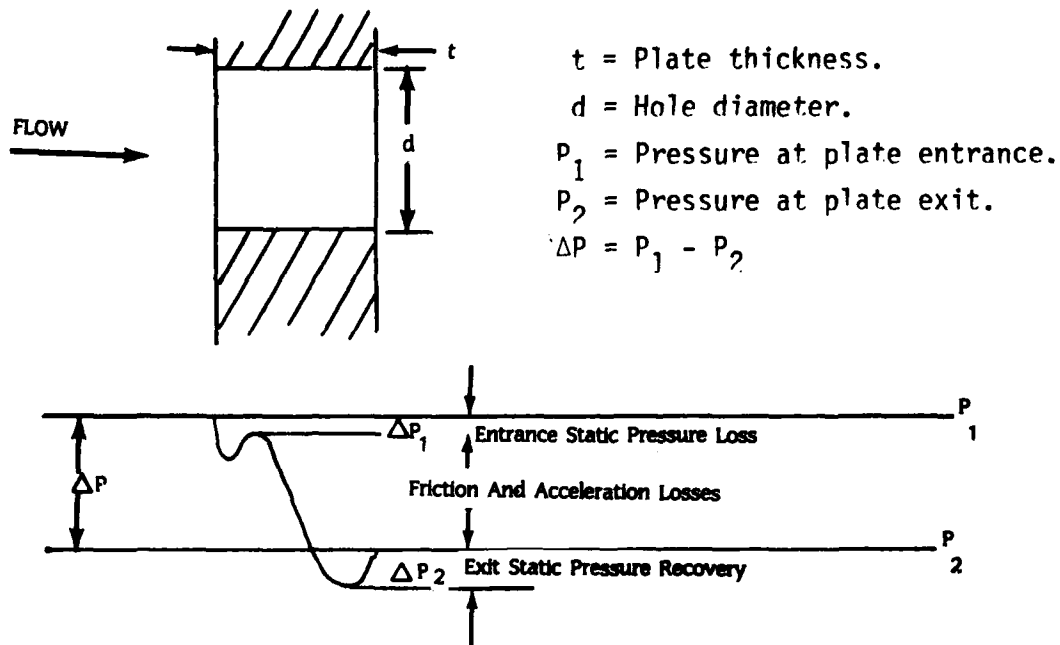


Figure C9. Plot of pressure drop across one plate

The change in pressure across the plate is a combination of entrance static pressure losses, friction and acceleration losses, and exit static pressure recovery for each hole. Equation (C30) quantifies these pressure changes as presented by Kays & London [3].

$$\frac{\Delta P}{P_1} = \frac{G^2 v_1}{2g_c P_1} [(1+K_c - \sigma^2)] + 2\left(\frac{v_2}{v_1} - 1\right) + f - \frac{A}{A_c} \frac{v_m}{v_1} - (1-K_e - \sigma^2) \frac{v_2}{v_1}$$

entrance acceleration friction exit (C30)
 loss loss loss regain

where

ΔP = Pressure drop across the plate.

P_1 = Pressure.

G = Flow stream mass velocity.

v = Specific volume.

g_c = Proportionality factor in Newton's second law.

K_c = Entrance coefficient as defined by Kays & London [3].

K_e = Exit coefficient as defined by Kays & London [3].

σ = Ratio of open area to frontal area.

A = Total heat-transfer area of one hole.

A_c = Minimum free flow area of one hole.

f = Mean friction factor in holes.

Subscripts

1 = Value at plane 1 (Figure C9).

2 = Value at plane 2 (Figure C9).

m = Average value.

The friction factor (f') is defined by the following relationship. This observed friction factor includes entrance and exit losses.

$$\Delta P = f' \frac{G^2 L}{2g_c \rho_m r_h}$$

where

ρ = fluid density.

L = Length of test section.

$r_h = A_c L / A$ = hydraulic radius.

Since only one plate is being considered, the total length of the exchanger is just the thickness of a plate ($L = t$).

$$\Delta P = \frac{G^2 v_m}{2g_c} f' \frac{A}{A_c} \quad (C31)$$

$$\Delta P = \frac{G^2 v_1}{2g_c} f' \frac{A}{A_c} \frac{v_m}{v_1}$$

Equating equations (C30) and (C31) results in a relationship for the observed friction factor per plate:

$$f' = \frac{[(1+K_c \sigma^2) + 2(v_2/v_1 - 1) - f(A/A_c)_{\text{hole}}(v_m/v_1) - (1-\sigma^2 - K_e)v_2/v_1]}{(A/A_c)_{\text{plate}} (v_m/v_1)} \quad (C32)$$

The hydraulic diameter is related to the hydraulic radius and A_c/A :

$$\frac{D_h}{L} = \frac{4r_h}{L} = \frac{4}{A} \frac{A_c}{A}$$

Rearranging this results in the following relationship for A/A_c :

$$\frac{A}{A_c} = \frac{4L}{D_h} \quad (C33)$$

For any circular cylinder, the diameter of the cylinder is the hydraulic diameter, and L is the plate thickness when only one plate is considered. Substituting these values in equation (C33) and substituting equation (C33) in equation (C32) results in the following equation for the observed friction factor for one plate:

$$f' = \frac{[(1+K_c-\sigma^2) + 2(v_2/v_1 - 1) - 4f(t/d)(v_m/v_1) - (1-\sigma^2 - K_e)(v_2/v_1)]}{(A/A_c)_{\text{plate}} (v_m/v_1)} \quad (C34)$$

To determine the friction factor as a function of hole Reynolds number, the various components of equation (C34) must be determined. First, $(A/A_c)_{\text{plate}}$ will be determined using the plate model.

$$A/A_c = A/A_{fr}$$

where

A_{fr} = Total frontal area.

A = Total heat-transfer surface area.

D = Diameter of test section.

Let

A_x = Area of hexagon around the hole.

A_o = Area of the hole.

$\alpha = \frac{\text{Total surface area of connected voids}}{\text{Total volume of matrix}}$

= area density (see Figure C1).

The area density definition is used to find the area density as a function of hole geometry and plate open area.

$$\begin{aligned} \alpha &= \frac{2[A_x - A_0] + 2\pi r t}{A_x t} \\ &= \frac{2}{t} \left[1 - \frac{A_0}{A_x}\right] + \frac{4\pi r t}{3\sqrt{3} b^2 t} \\ &= \frac{2}{t} (1-\sigma) + \frac{2\sigma}{r} \end{aligned}$$

Let A' and A'_c be the areas corresponding to a single hole.

$$\begin{aligned} A' &= \alpha A_x t = \alpha t A_0 / \sigma \\ &= \left[\frac{2}{t} (1-\sigma) + \frac{2\sigma}{r} \right] \left(\frac{\pi r^2}{\sigma} \right) t \end{aligned}$$

$$A'_c = \pi r^2$$

$$\frac{A}{A_c} = \frac{A'}{A'_c} = 2 \left[\frac{(1-\sigma)}{\sigma} + \frac{t}{r} \right] \quad (C.35)$$

Next, find v_2/v_1

For a perfect gas $v = \frac{RT}{P}$.

$$\frac{v_2}{v_1} = \frac{T_2 P_1}{T_1 P_2}$$

Let

ΔP = The pressure drop across a single plate.

n = Number of plates.

Then

$$\frac{\Sigma \Delta P}{n} = \text{Average pressure drop/plate.}$$

For a given plate the pressures can be related to the average pressure drop per plate.

$$P_2 = P_1 - \frac{\Sigma \Delta P}{n}$$

$$P_2/P_1 = 1 - \frac{\Sigma \Delta P}{nP_1}$$

Now, for any reasonable design, the pressure drop across the whole heat exchanger will be less than five percent, and there will be more than ten plates; so, for a reasonable design $P_2/P_1 \cong 1$ because

$$\frac{\Sigma \Delta P}{nP_1} \leq 0.005$$

Since

$$P_2/P_1 \cong 1$$

$$\frac{v_2}{v_1} = \frac{T_2}{T_1}$$

The same reasoning is used to find T_2/T_1 .

Let

ΔT = Temperature drop across an exchanger having n plates.

$$T_2 = T_1 \pm \frac{\Delta T}{n}$$

$$T_2/T_1 = 1 \pm \frac{\Delta T}{nT_1}$$

If the stream is being heated $T_2/T_1 \geq 1$ and if it is being cooled $T_2/T_1 \leq 1$ so, v_2/v_1 can have two values:

$$v_2/v_1 = 1 \pm \frac{\Delta T}{nT_1} \quad (C36)$$

v_m is the mean specific volume. v_m/v_1 can be found the same way v_2/v_1 was found.

$$v_m/v_1 = (T_m/T_1) (P_1/P_m)$$

$$P_1/P_m \cong 1$$

$$T_m = T_1 \pm \frac{\Delta T}{2n}$$

$$T_m/T_1 = 1 \pm \frac{\Delta T}{2nT_1}$$

$$v_m/v_1 = 1 \pm \frac{\Delta T}{2nT_1} \quad (C37)$$

Because of temperature variations along the length of the exchanger, the value of v_2/v_1 , and therefore f' , will vary from plate to plate. Average values of v_2/v_1 and v_m/v_1 will be used. When these values are applied to one plate and multiplied by the number of plates in the exchanger, the resulting total pressure drop will be the pressure drop measured over the whole exchanger.

$$\frac{\Delta T}{nT_1 |_{av}} = \frac{1}{\Delta T} \int_{T_{o1}}^{T_{o2}} \frac{\Delta T}{T_1} dT_1$$

$$\frac{\Delta T}{nT_1 |_{av}} = \frac{1}{n} \ln \frac{T_{o2}}{T_{o1}} \quad (C38)$$

where

- T_{o2} = Temperature exiting heat exchanger.
- T_{o1} = Temperature entering heat exchanger.
- $\Delta T = T_{o2} - T_{o1}$
- T_1 = Temperature at the inlet of any given plate

The average values of v_2/v_1 and v_m/v_1 follow:

$$v_2/v_1 |_{av} = 1 + \frac{1}{n} \ln \frac{T_{o2}}{T_{o1}} \quad (C39)$$

$$v_m/v_1 |_{av} = 1 + \frac{1}{2n} \ln \frac{T_{o2}}{T_{o1}} \quad (C40)$$

Next, the relationship between the calculated friction factor and the theoretical friction factor must be found.

Let

f_e = Measured friction factor.

f' = Theoretical observed friction factor.

The measured friction factor calculated from the data is defined as follows:

$$f_e = \frac{D_h \Delta P \rho_m g_c}{2nt G^2} \quad (C41)$$

Also, the following theoretical relationship exists for ΔP over one plate:

$$\Delta P = \frac{G^2 v_m}{2g_c} f' \frac{A}{A_c} \quad (C42)$$

Substitute equation (C42) in equation (C41). Equation (C42) is the pressure change over one plate so $n = 1$ for equation (C41). The Reynolds number is based on the hole diameter so $D_h = d$.

$$f_e = \frac{d}{2t} \left(\frac{G^2 v_m}{2g_c} f' \frac{A}{A_c} \right) \frac{g_c}{v_m G^2}$$

$$f_e = \frac{d}{4t} f' \frac{A}{A_c} \quad (C43)$$

Substituting equation (C34) into equation (C43) results in the following expression to theoretically estimate the measured friction factor:

$$f_e = \frac{(d/4t)(v_1/v_m) \left[(1+K_c - \sigma^2) + 2(v_2/v_1 - 1) + 4f(t/d)(v_m/v_1) - (1 - \sigma^2 - K_e)(v_2/v_1) \right]}{1} \quad (C44)$$

The test to determine the friction factor was performed at steady state room temperature. To compare the theoretical values with the experimental values, the following relationships will be used:

$$T_{o2}/T_{o1} = v_m/v_1 = v_2/v_1 = 1$$

For these conditions, equation (C44) becomes

$$f_e = \frac{d}{4t} (K_c + K_e) + f .$$

The friction factor per plate is a function of plate geometry and entrance, exit, and flow conditions in the hole. Kays and London present K_c and K_e in Figure 5-2 [3] and f in Figure 6-22 [3]. In both Tables the Reynolds number (N_R) is based on the hole diameter so, the hole Reynolds number (N_{Re}) is the same as N_R .

Table C1 presents the friction factors per plate for both punched and etched plates calculated using equation (C44). Table C2 presents the theoretical friction factors for the ERD plates.

Plate Description	N_{Re}	$N_{Re}(d/t)$	* fN_{Re}	$4(t/d)/N_{Re}$	** K_c	** K_e	f_e
Punched Plates d = 0.018" t = 0.021" $\sigma = 0.236$	10	8.571	16	0.467	0.97	0.45	1.9
	20	17.14	18	0.233	0.97	0.46	1.2
	50	42.86	21	0.093	0.91	0.46	0.71
	100	85.71	25	0.047	0.78	0.47	0.52
	200	171.43	32	0.023	0.75	0.48	0.42
Etched Plates d = 0.0285" t = 0.018" $\sigma = 0.09$	10	15.83	17	0.253	1.2	0.76	2.5
	20	31.67	20	0.126	0.97	0.76	1.7
	50	79.17	24	0.051	0.83	0.78	1.1
	100	158.3	30	0.025	0.80	0.79	0.93
	200	316.7	38	0.013	0.73	0.79	0.79
Etched Plates d = 0.0295" t = 0.0185" $\sigma = 0.245$	10	15.95	18	0.251	0.98	0.43	2.4
	20	31.89	21	0.125	0.97	0.43	1.6
	50	79.73	25	0.050	0.80	0.44	0.99
	100	159.46	31	0.025	0.70	0.48	0.78
	200	318.92	38	0.013	0.65	0.48	0.64

* Read from Kays and London, Table 6-22 [3].

** Read from Kays and London, Table 5-2 [3].

Table C1. Theoretical friction factor for punched and etched plates

Plate Description	N_{Re}	$N_{Re}(d/t)$	* fN_{Re}	$4(t/d)/N_{Re}$	** K_c	** K_e	f_e
d = 0.010" t = 0.065"	10	1.54	16	2.6	0.99	0.50	1.66
	20	3.08	16	1.3	0.99	0.50	0.86
	50	7.69	17	0.52	0.99	0.50	0.40
	100	15.38	19	0.26	0.99	0.50	0.25
	200	30.77	20	0.13	0.93	0.50	0.16
d = 0.010" t = 0.045"	10	2.22	16	1.8	0.99	0.50	1.68
	20	4.44	16	0.90	0.99	0.50	0.88
	50	11.11	18	0.36	0.99	0.50	0.44
	100	22.22	19	0.18	0.98	0.50	0.27
	200	44.44	22	0.09	0.93	0.50	0.19
d = 0.015" t = 0.065"	10	2.31	16	1.73	0.99	0.50	1.69
	20	4.62	16	0.867	0.99	0.50	0.89
	50	11.54	18	0.347	0.99	0.50	0.45
	100	23.08	19	0.173	0.98	0.50	0.28
	200	46.15	22	0.087	0.93	0.50	0.19
d = 0.020" t = 0.065"	10	3.08	16	1.3	0.99	0.50	1.71
	20	6.15	17	0.65	0.99	0.50	0.96
	50	15.38	19	0.26	0.99	0.50	0.49
	100	30.77	20	0.13	0.93	0.50	0.31
	200	61.54	24	0.065	0.82	0.51	0.22
d = 0.015" t = 0.045"	10	3.33	16	1.2	0.99	0.50	1.72
	20	6.67	17	0.60	0.99	0.50	0.97
	50	16.67	19	0.24	0.98	0.50	0.50
	100	33.33	20	0.12	0.93	0.50	0.32
	200	66.67	24	0.06	0.82	0.52	0.23
d = 0.020" t = 0.045"	10	4.44	16	0.90	0.99	0.50	1.77
	20	8.88	18	0.45	0.99	0.50	1.07
	50	22.22	19	0.18	0.98	0.50	0.54
	100	44.44	22	0.09	0.93	0.50	0.38
	200	88.89	26	0.045	0.80	0.53	0.28

* Read from Kays and London, Table 6-22 [3].

** Read from Kays and London, Table 5-2 [3].

Table C2. Theoretical friction factor for EBD plates 20% open area

Plate Description	N_{Re}	$N_{Re}(d/t)$	* fN_{Re}	$4(t/d)/N_{Re}$	** K_c	** K_e	f_e
$d = 0.010"$ $t = 0.020"$	10	5.00	17	0.80	0.99	0.50	1.89
	20	10.00	18	0.40	0.99	0.50	1.09
	50	25.00	20	0.16	0.96	0.50	0.58
	100	50.00	23	0.08	0.90	0.50	0.41
	200	100.00	28	0.040	0.80	0.54	0.31
$d = 0.015"$ $t = 0.020"$	10	7.50	17	0.533	0.99	0.50	1.98
	20	15.00	19	0.267	0.98	0.50	1.23
	50	37.50	21	0.107	0.93	0.50	0.69
	100	75.00	25	0.053	0.80	0.53	0.50
	200	150.00	30	0.027	0.75	0.54	0.39

* Read from Kays and London, Table 6-22 [3].

** Read from Kays and London, Table 5-2 [3].

Table C2. Concluded

4. DETERMINE N_{tu}/Plate vs HOLE REYNOLDS NUMBER

Once the N_{tu}/plate is found as a function of Reynolds number, the Colburn modules can be calculated using equation (1). The N_{tu}/plate was used to compare the experimental and theoretical results.

$$N_{tu} = \frac{UA}{\dot{m}c_p} \tag{C45}$$

where

- U = Overall thermal conductance.
- A = Total heat-transfer area.
- \dot{m} = Mass flow rate.
- c_p = Specific heat of fluid.

To find UA, divide the total heat-transfer area into three parts: the front face, the cylindrical hole, and the back face. Once the area averaged heat-transfer coefficient is found for each area, UA can be found from the following relationship

$$UA = h_1 A_1 + h_2 A_2 + h_3 A_3$$

Where h = Area averaged heat-transfer coefficient.

Subscripts

1 = Front face.

2 = Cylindrical hole.

3 = Back face.

UA can be approximated by assuming the front and back surfaces have the same heat-transfer characteristics.

$$UA = 2h_1 A_1 + h_2 A_2 \quad (C46)$$

A_1 is the solid surface of the plate, which is the frontal area times the percent solid area.

$$A_1 = A_{fr} (1 - \sigma) \quad (C47)$$

The total heat-transfer area, A, can be found by manipulating equation (C35).

$$\frac{A}{A_c} = 2 \left[\frac{1-\sigma}{\sigma} + \frac{t}{r} \right] \quad (C35)$$

$$A = 2 \left[\frac{1-\sigma}{\sigma} + \frac{2t}{d} \right] A_c \left(\frac{A_{fr}}{A_c} \right)$$

$$A = 2A_{fr} \left[1 - \sigma + \frac{2t\sigma}{d} \right] \quad (C48)$$

A_2 can be found from the following relationship:

$$A = 2A_1 + A_2 \quad (C49)$$

$$\begin{aligned} A_2 &= A - 2A_1 \\ &= 2A_{fr} \left[1 - \sigma \frac{2t\sigma}{d} \right] - 2A_{fr}(1-\sigma) \end{aligned}$$

$$A = \frac{4A_{fr}t\sigma}{d} \quad (C50)$$

Next, find an expression for $\dot{m}c_p$ as a function of hole Reynolds number.

$$\begin{aligned} \dot{m}c_p &= \dot{m}c_p \frac{(N_{Re}\mu)(\rho A_c V)}{\rho V D} \left(\frac{\sigma A_{fr}}{A_c} \right) \\ \dot{m}c_p &= \frac{N_{Re}\mu\sigma A_{fr}c_p}{d} \quad (C51) \end{aligned}$$

where

- N_{Re} = Hole Reynolds number.
- μ = Viscosity.
- ρ = Fluid density.
- V = Fluid velocity upstream of test section.
- D = Diameter of tubing upstream of test section.
- A_c = Open area of plate.
- σ = Ratio of open area to plate frontal area.
- A_{fr} = Frontal area of plate.
- d = Hole diameter.

Now, substitute equations (C47), (C41), and (C51) in equation (C46).

$$N_{tu} = \frac{\{h_1[2A_{fr}(1-\sigma)] + h_2(A_{fr}\sigma t/d)\}d}{N_{Re}\mu\sigma A_{fr}c_p}$$

$$N_{tu} = \frac{1}{N_{Re}\mu c_p} \frac{[2h_1 d(1-\sigma) + 4h_2 t]}{\sigma} \quad (C52)$$

Now it's necessary to find h_1 and h_2 . h_1 can be found as a function of the upstream mass velocity (before the flow enters the plate), G' , and the equivalent cylinder diameter, d' . Due to continuity, the upstream mass velocity is related to the mass velocity in the core as follows:

$$G' = G\sigma \quad (C53)$$

The equivalent cylinder diameter can be approximated by the following equation:

$$d' = 2y(x)|_{av} \quad (C54)$$

Note that $y(x)$ is shown on Figure C6.

$$\frac{d'}{d} = \frac{2y(x)|_{av}}{d} = \frac{y(x)|_{av}}{r} \quad (C55)$$

Substitute equation (C24) for $y(x)|_{av}$ in equation (C55), then replace r/b with equation (C26):

$$\frac{d'}{d} = \left[\frac{\sqrt{3}/2}{0.9094\sigma^{1/2}\cos\theta} - 1 \right]_{av}$$

Integrate over one 12th of a hole to find d'/d :

$$\frac{d'}{d} = \frac{6}{\pi} \int_0^{\pi/6} \left(\frac{0.952}{\sigma^{1/2} \cos \theta} - 1 \right) d\theta \quad (C56)$$

A relationship for d'/d as a function of σ can be approximated by correlating values evaluated using equation (C56). Equation (C57) is accurate to 10% of d'/d obtained by numerically integrating equation (C56) for $\sigma \leq 0.3$.

$$d'/d = .358 \sigma^{-.768} \quad (C57)$$

A relationship for h_1 (C58) is presented in McAdams' "Heat Transmission." [4] Although this relationship is based on data from air, it can be used for the helium heat exchangers because the Prandtl numbers are approximately equal. The relationship is also an approximation because equation (C58) is for flow normal to a single cylinder. This was used to approximate the flow normal to a flat plate because no reference could be found for low Reynolds number flow normal to a flat plate. Dr Fowle [1] believes this is a conservative estimate -- it will predict lower than actual $N_{tu}/plate$.

$$\frac{h_1 d'}{k} = 0.32 + 0.43 \left(\frac{d' G'}{\mu} \right)^{0.52} \quad (C58)$$

$$\text{for } 0.1 \leq \frac{d' G'}{\mu} \leq 1000$$

Note the following relationship for the Reynolds number:

$$\frac{dG}{\mu} = N_{Re} \quad (C59)$$

Substituting equations (C53), (C57), and (C59) in equation (C58) results in the following expression for h_1 :

$$h_1 = (k/d) 2.793 \sigma^{0.768} [0.32 + 0.252 N_{Re}^{0.52} \sigma^{0.121}] \quad (C60)$$

Two equations (C61 and C62) to calculate h_2 are shown in "Heat, Mass and Momentum Transfer" by Robsenow and Choi [5]. These functions are for heat transfer in a circular cylinder and are based on the following assumptions:

$$1 \leq N_{Re} \leq 1000$$

$$N_{Pr} = 0.7$$

(Uniform wall temperature)

The first expression for h_2 assumes a developing velocity profile in laminar flow.

$$h_2 = k/d \left[3.66 + \frac{0.073 d/t N_{Re}}{1 + 0.012 (d/t N_{Re})^{0.8}} \right] \quad (C61)$$

The second expression for h_2 assumes a parabolic velocity profile in laminar flow.

$$h_2 = k/d \left[3.66 + \frac{0.047 (d/t N_{Re})}{1 + 0.032 (d/t N_{Re})^{0.667}} \right] \quad (C62)$$

Substituting equations (C60), (C61), and (C62) in equation (C52) and recognizing that

$$N_{Pr} = \frac{\mu c_p}{k} = 0.7$$

results in equations (C63) and (C67).

FOR A DEVELOPING VELOCITY PROFILE IN LAMINAR FLOW

$$N_{tu}/\text{Plate} = \quad (C63)$$

$$\frac{(1-\sigma)\sigma^{-0.232} (2.554+2.011 N_{Re}^{0.52} \sigma^{0.121}) + 20.9 t/d + 0.417}{N_{Re} + N_{Re} [1+0.012(d/t N_{Re})^{0.8}]}$$

For the punched plate ($d = 0.18"$, $t = 0.021"$, $\sigma = 0.236$)

$$N_{tu}/\text{plate} = 27.1 N_{Re}^{-1} + 1.803 N_{Re}^{-0.48} + \frac{0.416}{1 + 0.011 N_{Re}^{0.8}} \quad (C64)$$

For the etched plates ($d = 0.0285"$, $t = 0.0185"$, $\sigma = 0.09$)

$$N_{tu}/\text{plate} = 17.63 N_{Re}^{-1} + 2.391 N_{Re}^{-0.48} + \frac{0.417}{1 + 0.017 N_{Re}^{0.8}} \quad (C65)$$

For the etched plates ($d = 0.0295"$, $t = 0.018"$, $\sigma = 0.245$)

$$N_{tu}/\text{plate} = 15.42 N_{Re}^{-1} + 1.775 N_{Re}^{-0.48} + \frac{0.417}{1 + 0.018 N_{Re}^{0.8}} \quad (C66)$$

FOR A PARABOLIC VELOCITY PROFILE IN LAMINAR FLOW

$$N_{tu}/plate = \quad (C67)$$

$$\frac{(1-\sigma)^{-0.232} (2.554 + 2.011 N_{Re}^{0.52} \sigma^{0.121})^{20.9} t/d^{0.269}}{N_{Re}} + \frac{0.269}{N_{Re}} + \frac{0.269}{1 + 0.032 (d/t N_{Re})^{0.667}}$$

For the punched plate

$$N_{tu}/plate = 27.1 N_{Re}^{-1} + 1.803 N_{Re}^{-0.48} + \frac{0.269}{1 + 0.029 N_{Re}^{0.667}} \quad (C68)$$

For the etched plate (9% open area)

$$N_{tu}/plate = 17.63 N_{Re}^{-1} + 2.391 N_{Re}^{-0.48} + \frac{0.269}{1 + 0.043 N_{Re}^{0.667}} \quad (C69)$$

For the etched plate (24.5% open area)

$$N_{tu}/plate = 15.42 N_{Re}^{-1} + 1.775 N_{Re}^{-0.48} + \frac{0.269}{1 + 0.044 N_{Re}^{0.667}} \quad (C70)$$

Table C3 presents the predicted values of $N_{tu}/plate$ vs hole Reynolds number for the developing and parabolic velocity profiles in the punched and etched plates.

N _{tu} /plate						
Developing Velocity Profile				Parabolic Velocity Profile		
	Punched	Etched		Punched	Etched	
N _{Re}	σ =0.236	σ =0.09	σ =0.245	σ =0.236	σ =0.09	σ =0.245
10	3.697	2.931	2.505	3.544	2.779	2.353
20	2.155	1.801	1.541	2.005	1.654	1.395
50	1.151	1.019	0.876	1.011	0.818	0.748
100	0.759	0.687	0.593	0.634	0.578	0.486
200	0.514	0.468	0.403	0.412	0.385	0.323
500	0.307	0.277	0.238	0.241	0.229	0.191

Table C3. N_{tu}/plate vs hole Reynolds number for the punched and etched plates

The parabolic velocity profile generated N_{tu}/plate values closest to the experimental results. Consequently, a parabolic velocity profile was used to compare the theoretical and experimental results. Table C3 presents the N_{tu}/plate vs N_{Re} calculated using equations (C56), (C52), (C58), and (C62). Instead of using equation (C57) which estimates d'/d as a function of σ, equation (C56) was numerically integrated to find values for d'/d. The theoretical results were correlated and b and m were found to make the following equation fit the theoretical results:

$$N_{tu}/plate = b(N_{Re})^m$$

Type of Plate	d/t	σ	N_{Re}	$N_{tu}/plate$	b	m
Electron Beam Drilled	0.154	0.20	10	14.785	116.63	-0.907
			20	7.654		
			30	5.253		
			40	4.043		
			50	3.311		
			60	2.820		
			70	2.467		
			80	2.201		
			90	1.992		
			100	1.824		
	0.222	0.20	10	10.600	77.78	-0.878
			20	5.558		
			30	3.853		
			40	2.991		
			50	2.467		
			60	2.115		
			70	1.861		
			80	1.669		
			90	1.518		
			100	1.396		
	0.231	0.20	10	10.251	74.62	-0.875
			20	5.383		
			30	3.736		
			40	2.903		
			50	2.397		
			60	2.056		
			70	1.810		
			80	1.624		
			90	1.478		
			100	1.360		

Table C4. Theoretical $N_{tu}/plate$ assuming a parabolic velocity profile

Type of Plate	d/t σ	N_{Re}	$N_{tu}/plate$	b	m
	0.308 0.20	10	7.982	54.39	-0.848
		20	4.246		
		30	2.976		
		40	2.330		
		50	1.937		
		60	1.671		
		70	1.479		
		80	1.333		
		90	1.218		
		100	1.125		
Electron Beam Drilled	0.333 0.20	10	7.458	49.86	-0.840
		20	3.983		
		30	2.800		
		40	2.198		
		50	1.830		
		60	1.582		
		70	1.402		
		80	1.265		
		90	1.157		
		100	1.070		
	0.444 0.20	10	5.886	36.62	-0.810
		20	3.194		
		30	2.271		
		40	1.798		
		50	1.509		
		60	1.312		
		70	1.169		
		80	1.060		
		90	0.973		
		100	0.903		

Table C4. Continued

Type of Plate	d/t σ	N_{Re}	$N_{tu}/plate$	b	m
	0.500 0.20	10	5.362	32.38	-0.798
		20	2.930		
		30	2.094		
		40	1.665		
		50	1.401		
		60	1.221		
		70	1.090		
		80	0.990		
		90	0.911		
		100	0.846		
	0.750 0.20	10	3.961	21.56	-0.754
		20	2.224		
		30	1.618		
		40	1.304		
		50	1.109		
		60	0.975		
		70	0.876		
		80	0.801		
		90	0.740		
		100	0.691		
Punched	0.857 0.236	10	3.562	18.87	-0.742
		20	2.016		
		30	1.474		
		40	1.192		
		50	1.017		
		60	0.896		
		70	0.807		
		80	0.738		
		90	0.683		
		100	0.638		

Table 4. Continued

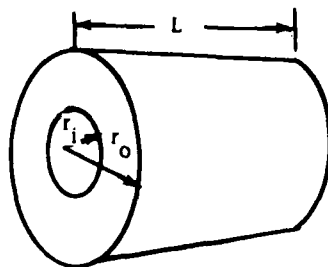
Type of Plate	d/t	σ	N_{Re}	$N_{tu}/plate$	b	m
Etched	1.583	0.09	10	2.725	12.41	-0.674
			20	1.624		
			30	1.224		
			40	1.010		
			50	0.874		
			60	0.779		
			70	0.708		
			80	0.652		
			90	0.607		
			100	0.570		
	1.595	0.245	10	2.410	11.15	-0.682
			20	1.426		
			30	1.071		
			40	0.882		
			50	0.762		
			60	0.679		
			70	0.616		
			80	0.567		
			90	0.528		
			100	0.495		

Table C4. Concluded

APPENDIX D - INSULATION REQUIREMENTS

When a heat leak was discovered in the test section, the insulation had to be changed to reduce the heat leak. Although a steady-state analysis had shown the insulation was adequate, a transient analysis showed that more insulation was needed. A comparison of the steady state and transient analyses follow.

1. STEADY STATE



L = Length of test section.

r_i = Radius of test section.

r_o = Radius of test section and insulation.

h_a = Natural convective heat-transfer coefficient.

k = Thermal conductivity of insulation.

T_i = Temperature inside cylinder.

T_a = Temperature outside cylinder.

Figure D1. Schematic of test section

The heat leak through the insulation can be calculated from the following equation:

$$\dot{q} = 2\pi r_i L (T_i - T_a) / U \quad (D1)$$

where

$$U = (1/h_a)(r_i/r_o) + (1/k)r_i \ln(r_o/r_i)$$

The following properties were used to generate a curve of q vs insulation thickness.

$$r_i = 1.5 \text{ in}$$

$$L = 4.2 \text{ in}$$

$$h_a = 1 \text{ BTU/hr ft}^2 \text{ F}$$

$$\Delta T = (T_i - T_a) = 20^\circ \text{F}$$

$$k = 0.025 \text{ BTU/ft hr F (polyurethane foam)}$$

Applying these conditions to equation (D1) results in the relationship shown in Figure D2.

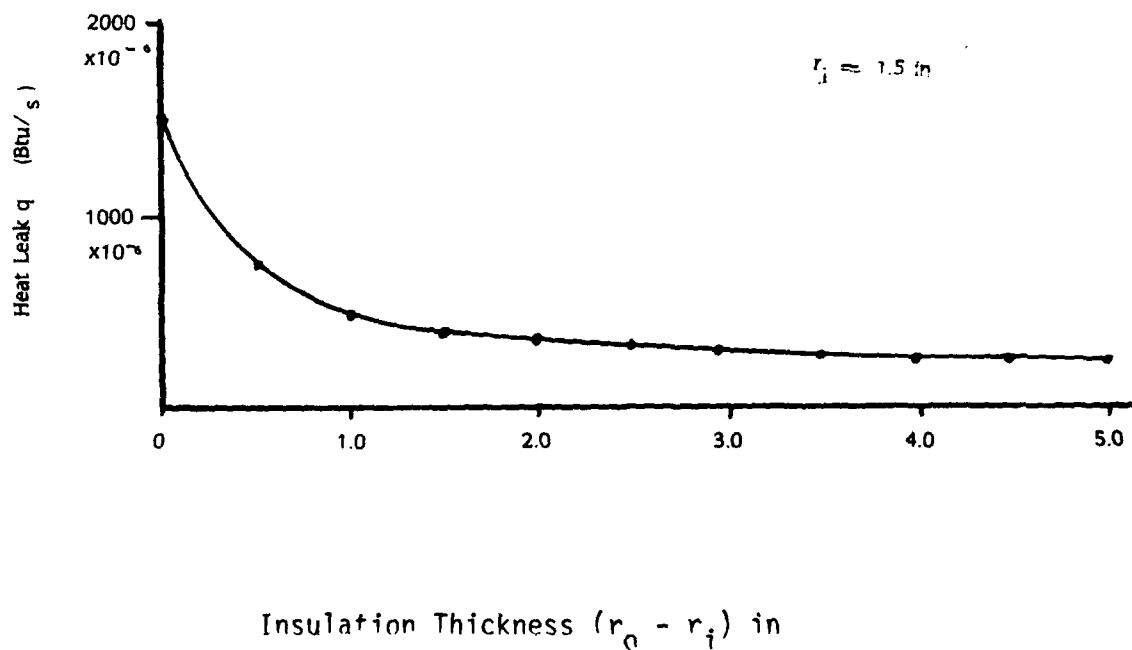
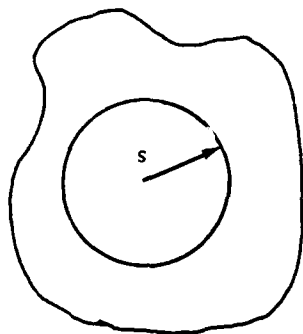


Figure D2. Plot of heat leak rate vs insulation thickness (steady-state analysis)

If $h_a r_i / k \geq 1$ adding insulation always decreases the heat leak. If $h_a r_i / k < 1$ there is an area where adding insulation increases the heat leak. In this case, the steady-state analysis shows that adding insulation would reduce the heat leak and that 1.5" of insulation was sufficient.

2. TRANSIENT THERMAL BEHAVIOR OF INSULATION



- k = Thermal conductivity of insulation.
- ρ = Insulation density.
- c = Specific heat of insulation.
- $\alpha = k/\rho c$ = thermal diffusivity.
- s = Radius of test section.
- l = Length of test section.
- Q_s = Total heat loss in time τ .
- θ_s = Temperature difference between heated core and ambient temperature.
- τ = Time, measured from test start.

Figure D3. Model of the insulated test section

The test section is modeled by a circular cylinder surrounded by an infinitely thick layer of insulation (Figure D3). The temperature at the surface of the pipe is instantaneously increased (θ_s) when the test starts ($\tau=0$). The dimensionless group $\alpha Q_s / k L s^2 \theta_s$ is tabulated as a function of $\alpha \tau / s^2$ by Jakob [6]; consequently, for a given time (τ) and insulator qualities (α), the total heat loss (Q_s) can be found.

The test section had the following properties:

$$\begin{aligned} s &= 0.125 \text{ ft} \\ \theta_s &= 20^\circ\text{F} \\ L &= 4.2/12 \text{ ft} \end{aligned}$$

Table D1 presents the three insulation cases that were evaluated.

	Case 1	Case 2	Case 3			
k (BTU/hr ft F)	0.03	0.02	0.025			
ρ (lbm/ft ³)	6	2	2.34			
c (BTU/lbm F)	0.33	0.33	0.33			
τ (sec)	$\frac{\alpha\tau}{s^2}$	$\frac{Q_s}{(BTU)}$	$\frac{\alpha\tau}{s^2}$	$\frac{Q_s}{(BTU)}$	$\frac{\alpha\tau}{s^2}$	$\frac{Q_s}{(BTU)}$
20	0.00533	0.116	0.011	0.055	0.012	0.0667
40	0.011	0.166	0.021	0.079	0.023	0.0952
60	0.016	0.204	0.032	0.097	0.035	0.1177
80	0.021	0.238	0.043	0.114	0.046	0.1383
100	0.027	0.264	0.053	0.130	0.058	0.1567
200	0.053	0.389	0.107	0.190	0.115	0.2290
300	0.080	0.483	0.160	0.237	0.173	0.2883
400	0.107	0.571	0.213	0.282	0.230	0.3396
500	0.133	0.642	0.267	0.318	0.288	0.3855

Table D1. Comparison of different insulation requirements

Figure D4 compares insulation with various kpc products. The analysis indicates that total heat loss decreases as the kpc product decreases. Also, no insulation causes a smaller heat leak than an infinite amount of insulation for short runs. During most of the test runs the core reached steady state in 90 to 660 seconds; only one run was under 90 seconds. The modified apparatus used 3" of insulation with a kpc product of $0.019 \text{ BTU}^2/\text{hr ft}^4 \text{ F}$ (case 3).

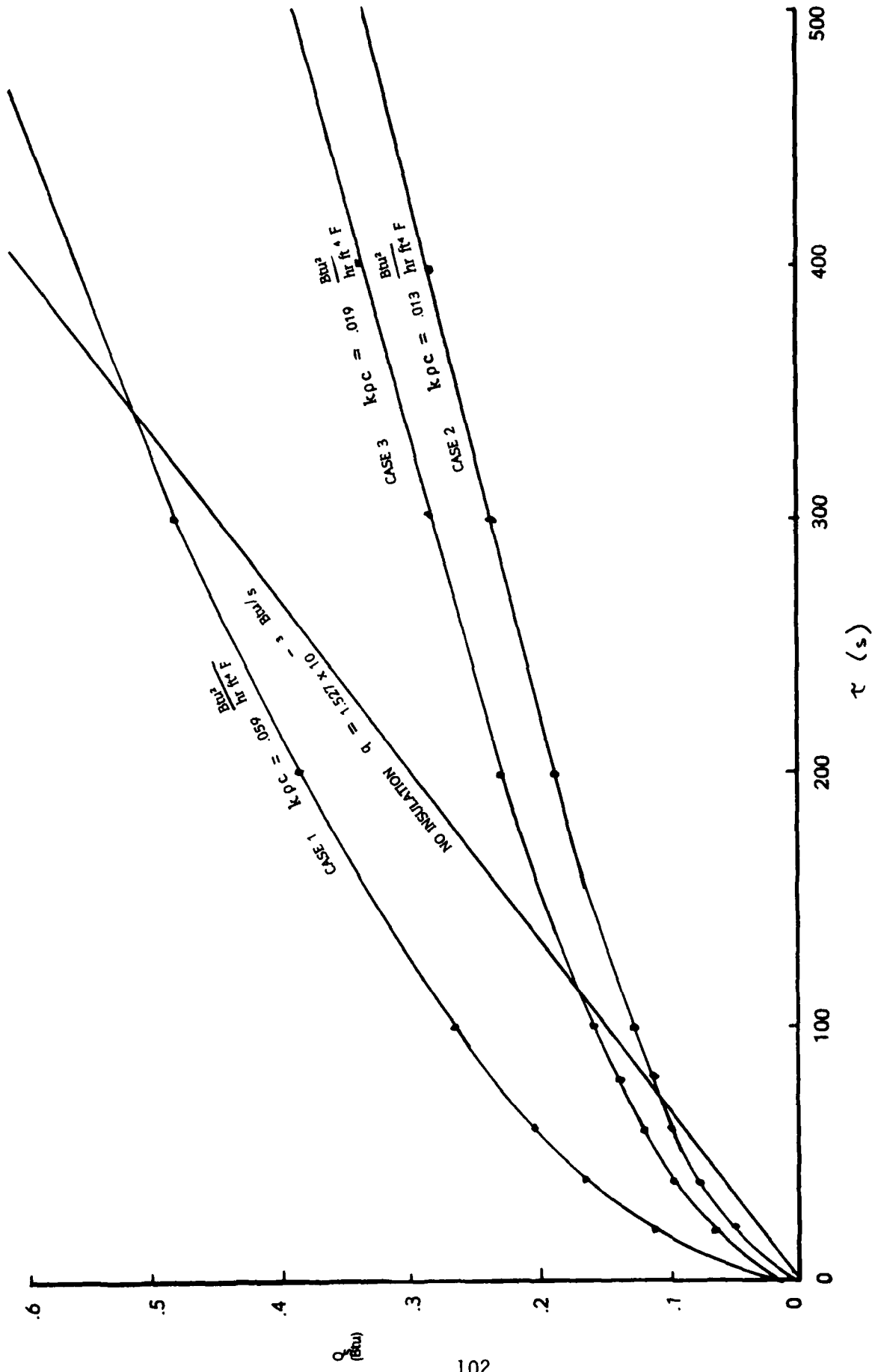


Figure D4. Transient analysis of heat loss for an infinite thickness of insulation

REFERENCES

1. R.H. Hubbell, Summary Report on Task no. 31, Determination of f and j Data for Perforated Plates, Development of an Advanced Two-Stage Rotary Reciprocating Refrigerator, Air Force Wright Aeronautical Laboratories, Flight Dynamics Laboratory, Wright-Patterson Air Force Base, Ohio 45433-6553, Contract no. F33615-81-C-3419, Project no. 2126, June 1984.
2. P.F. Pucci, C.P. Howard, C.H. Piersall, Jr., "The Single-Blow Transient Testing Technique for Compact Heat Exchanger Surfaces," Journal of Engineering for Power, January 1967, pp. 29-40.
3. W.M. Kays, and A.L. London, Compact Heat Exchangers, 2nd Edition, McGraw Hill, New York, 1964.
4. McAdams, Heat Transmission, 3rd Edition, McGraw-Hill, New York, 1954, p260.
5. Rohsenow and Choi, Heat, Mass, and Momentum Transfer, Prentice Hall, 1961, p 166.
6. M. Jakob, Heat Transfer Vol I, Wiley and sons, Inc., New York, 1950, p267.